Unambiguous identification of N-containing oxygenated organic molecules using CI-Orbitrap in an eastern Chinese megacity

Yiqun Lu[1,2], Yingge Ma[1], Dan Dan Huang[1], Shengrong Lou[1], Sheng'ao Jing[1], Yaqin Gao[1], Hongli Wang[1], Yanjun Zhang[3], Hui Chen[4], Yunhua Chang[5], Naiqiang Yan[2], Jianmin Chen[4], Christian George[3], Matthieu Riva[3], Cheng Huang[1]*

[1] State Environmental Protection Key Laboratory of Formation and Prevention of Urban Air Pollution Complex, Shanghai Academy of Environmental Sciences, Shanghai 200233, China;

[2] School of Environmental Science and Engineering, Shanghai Jiao Tong University, Shanghai 200240, China

[3] Univ. Lyon, Université Claude Bernard Lyon1, CNRS, IRCELYON, 69626 Villeurbanne, France;

[4] Shanghai Key Laboratory of Atmospheric Particle Pollution and Prevention (LAP[3]), Department of Environmental Science & Engineering, Jiangwan Campus, Fudan University, Shanghai 200438, China

[5] Collaborative Innovation Center on Forecast and Evaluation of Meteorological Disasters (CIC-FEMD), NUIST Center on Atmospheric Environment, Nanjing University of Information Science and Technology, Nanjing 210044, China

Corresponding authors: Cheng Huang (huangc@saes.sh.cn)

ABSTRACT

Oxygenated organic molecules (OOMs) are dominated by the N-containing species in polluted urban environment. As N-containing OOMs, especially those with more than one nitrogen atoms, prevailed in the high m/z range (m/z > 350Th), unambiguous identification of N-containing OOMs is highly desirable for understanding of their formation processes, precursors and influencing factors. To achieve this, we applied an ultra-high-resolution chemical ionization-orbitrap (CI-Orbitrap) in a field campaign and found that OOMs contain one (1N-OOMs), two (2N-OOMs) and three (3N-OOMs) nitrogen atoms respectively comprised 50%, 26% and 4% of total OOMs. More interestingly, the fraction of 2N-OOMs increased with the increase of carbon number (nC) and were dominated by the ones derived from aliphatic precursors (2N-OOM_{Ali}, 64.2%), indicating the importance of multistep oxidation. Plausible precursors of 2N-OOMs were aliphatics (2N-OOM_{Ali}, 64.2%), aromatics (2N-OOM_{Aro}, 16%), and monoterpenes (2N-OOM_{MT}, 15.4%). The absolute concentrations of 2N-OOMs were greatly affected by the pollution level for the most cases. The 2N-OOM_{Ali} was the most abundant 2N-OOMs and its fraction even increased in the polluted day with enhanced proportion of the ones with nC>10. While 2N-OOM_{Ali} and 2N-OOM_{Aro} were dominated by daytime photochemical production, nighttime NO_3-initiated oxidation played a comparable role as the daytime photochemistry in the formation of 2N-OOM_{MT}. 2N-OOM_{Aro} were of highest oxygenation level, followed by 2N-OOM_{MT} and 2N-OOM_{Ali}, which were affected by photochemistry and NO_x concentrations. These results highlight the significant formation of 2N-OOMs and the influencing factors, on their formation in polluted urban environment, where various VOC precursors and atmospheric oxidants present.

1. Introduction

Secondary organic aerosol (SOA) accounts for a significant fraction of particulate matters (Donahue et al., 2009; Ehn et al., 2014; Hallquist et al., 2009; Jimenez et al., 2009). Volatile organic compounds (VOCs) and their oxidation products, *i.e.*, OVOCs, are important precursors of SOA in the atmosphere (Atkinson and Arey, 2003; Bianchi et al., 2019; Ehn et al., 2014; Nie et al., 2022). The N-containing oxygenated organic molecules (OOMs) have been identified as the important products upon VOC oxidation. Especially at high NO_x levels, these products become more dominant while the others (*i.e.*, alcohols, hydroperoxides and RO_2 cross-reaction products) are likely suppressed (Bianchi et al., 2019; Zhao et al., 2018). The nitrogen atoms in OOM molecules are assumed to be mainly associated with nitrate group ($-ONO_2$) formed from bi-molecular reaction between RO_2 radical and NO. Field measurements also observed that up to 77 % of molecules in organic aerosol (OA) contain nitrate functional groups under different atmospheric conditions (Ditto et al., 2020; Kenagy et al., 2021; Kiendler-Scharr et al., 2016; Lee et al., 2016; Lee Ng et al., 2017; Lin et al., 2021; Rollins et al., 2013; Xu et al., 2015; Ye et al., 2021; Yu et al., 2019).

The N-containing OOM molecules can be classified into 1N-OOMs, 2N-OOMs, and 3N-OOMs, according to the number of N atoms in the molecule. The chemical composition of N- containing OOMs is determined by their precursors, formation pathways and NO_x level in the atmosphere (Bianchi et al., 2019; Ehn et al., 2014; Nie et al., 2022; Pye et al., 2019; Riva, 2016; Yan et al., 2016). Recent observations in megacities of China indicated that 2N-OOMs accounted for significant fractions (about 30-33%) among total N-containing OOMs besides 1N-OOMs (66-70%) due to the high NO_x concentrations in polluted urban environment (Nie et al., 2022; Yan et al., 2021). Some laboratory studies also proposed that the potential formation pathways of 2N-OOMs, such as the multiple-step OH oxidation (Garmash et al., 2020) or the NO_3-initiated oxidation followed by NO termination (Kiendler-Scharr et al., 2016; Liebmann et al., 2019), suggesting the increased importance of multi-step bimolecular oxidation in the formation of 2N-OOMs. On the other hand, it was also found that the formation of 2N-OOMs showed the clear preference of specific precursors compared to 1N-OOMs, *i.e.*, significantly higher branch ratio of 2N-OOMs from

aliphatic hydrocarbons than those from aromatics (Nie et al., 2022), suggesting considerable difference from 1N-OOMs in terms of formation pathway. Determining the formation pathway of N-containing OOM molecules, especially those containing two to three nitrogen atoms, in real atmosphere, is challenging. Identification of their chemical compositions in molecular level is the key for advancing our understanding in the precursor, formation and sources of N-containing OOMs in polluted atmosphere, where thousands of oxidation products exist and evolve constantly.

Traditionally, a chemical ionization atmospheric pressure interface time-of-flight mass spectrometer (CI-APi-TOF) has been used to measure the gaseous OOMs (Berndt et al., 2016; Ehn et al., 2014; Jokinen et al., 2014; Rissanen et al., 2014). Using a CI-APi-TOF, increasing number of studies have been reporting the formation of OOMs through the oxidation of various VOC precursors in chamber or flow tube (Berndt et al., 2016, 2018; Ehn et al., 2014; Garmash et al., 2020; Jokinen et al., 2014, 2015; Rissanen et al., 2014; Wang et al., 2020; Zhao et al., 2018). While 2N-OOMs in real ambient almost exclusively located in high m/z (mass-to-charge) range (*i.e.*, 300 - 500 Th), a CI-APi-TOF with highest mass resolving power of 12,000 (m/Δm, in full width at half maximum) at m/z=200 Th and above, can hardly identify the molecular compositions of 2N-OOMs unambiguously. This is because low mass resolving power imposes significant uncertainties on separating overlapping peaks, which increases rapidly with increasing m/z and decreasing mass resolving power. Taken the integer m/z of 342 as an example, multiple peaks overlap at this nominal mass, *i.e.*, $C_7H_8O_{10}N_2(NO_3)^-$ (342.0057 Th), $C_8H_{12}O_9N_2(NO_3)^-$ (342.0421 Th), $C_9H_{16}O_8N_2(NO_3)^-$ (342.0785 Th), $C_{10}H_{20}O_7N_2(NO_3)^-$ (342.1149 Th). The adjacent peaks are of mass differences (Δm) of 0.0364 and a good peak separation of these peaks (4σ) requires mass resolving power of at least 16,000. Therefore, development and application of mass spectrometry techniques with extremely high performance in detection limit, time resolution, and mass resolving power, are highly desirable.

To achieve accurate identification of molecular formula from the extremely complex mass spectra, a CI (nitrate) inlet had also been coupled to an orbitrap mass spectrometer (CI-Orbitrap) to measure the OOMs in ultra-high mass resolving power (m/Δm> 100,000 at m/z=200-500 Th) (Riva et al., 2019a; Zhang et al., 2022). The ultra-high mass resolving power of CI-Orbitrap will undoubtedly provide

significant improvements in molecular identification, separation, and quantification. Herein, we applied a CI-Orbitrap in a field campaign for the measurements of OOMs, with a special focus on 2N-OOMs, in molecular level in urban Shanghai. The site represents a typical eastern Chinese megacity characterized by intense human activities, multiple anthropogenic emissions and high NO_x concentrations. Based on the measurement results as well as our current knowledge on N-containing OOM formation, we classify the observed 2N-OOMs into different precursor groups and explore the potential influencing factors on their formation. Furthermore, supported by positive matrix factorization (PMF), sources and gas-phase oxidation processes for 2N-OOM formation in urban Shanghai were identified.

2. Ambient measurement and methodology

2.1 Measurements

The field campaign was carried out from 31th October to 18th November, 2020 on the top-floor of an 8-story building in Shanghai Academy of Environmental Sciences (31°18' N, 121°43' E, Figure S1), which sits in a densely populated region surrounded by commercial properties and residential dwellings without significant industrial sources nearby. The site can represent a typical urban area of Shanghai affected by severe local emissions from vehicular traffic, commercial, and residential activities. Our campaign was carried out in autumn which represents a typical transition period from strong photochemistry in summer to intense regional transport in winter. At times, air masses transported from the neighboring provinces or even further from the northern China can also affect the air quality of the site.

The 2N-OOMs as well other OOMs molecules were measured in real time with a nitrate-Orbitrap. The operation of nitrate-Orbitrap has been detailed in previous studies as well as in one of our companion studies (Zhang et al., 2022), thus is only briefly described here. Ambient air was drawn into the ionization source through a 1m stainless-steel tube (3/4 inch). The reagent ion was produced by passing nitric acid in sheath flow (20L/min) into a PhotoIonizer (Model L9491, Hamamatsu, Japan) and was then introduced into a co-axial laminar flow reactor, in which the reagent ions interact with the air samples. The charged species were detected by an orbitrap mass analyzer with a mass resolving power of about 140,000. Mass-dependent transmission calibrations was also performed using a depletion method (Heinritzi et al., 2016).

Other ancillary measurements, including the $PM_{2.5}$ concentrations, trace gases (SO_2, O_3 and NO_x), volatile organic compounds, as well as meteorological parameters (wind direction and speed, solar radiation, etc.) were detailed in Supporting Information (SI-1). An overview of the measurement data, illustrating the air quality as well as the meteorological conditions during the campaign, is provided in SI-2 and Figure S2.

2.2 Data analysis of nitrate CI-Orbitrap

The raw mass spectra were first extracted by Orbitool (Cai et al., 2020) and the molecular information was then achieved by applying a homemade toolkit based on the MATLAB software. The toolkit drew on the idea from "tofTools" package which is used for analyzing the mass spectral data obtained from the TOF analyzer, such as nitrate CI-API-TOF (Junninen et al., 2010). The concentrations of the detected species are then determined as follows:

$$[\boldsymbol{X}] = \frac{\boldsymbol{i}[\boldsymbol{X}^-]}{\boldsymbol{NO_3^-} \cdot (\boldsymbol{HNO_3})_{\boldsymbol{0-2}}} \cdot \boldsymbol{C} \quad (\mathbf{1})$$

where $i[X^-]$ is the transmission-corrected signal intensity of ion X in unit of counts per second (cps), C represents the calibration factor. C is determined from the collision frequency of target species with the nitrate ions (cluster) during its residence in the charger, taking into account of the losses onto the walls of the reactor and the tube (Eq. 2):

$$\boldsymbol{C} = \boldsymbol{C_{H2SO4}} = \frac{\mathbf{1}}{\boldsymbol{k_{ion}} \times \boldsymbol{RT} \times \boldsymbol{f_{inlet}}} \quad (\mathbf{2})$$

where k_{ions} is the ion collision frequency in the range of (1.7 – 2.3) $\times 10^{-9}$ cm^3 s^{-1} (Ehn et al., 2014); RT is the residence time in the charger and f_{inlet} represents the fractions of target species that passed through the inlet.

Herein, we apply the C determined for sulfuric acid (H_2SO_4) of 3.4×10^9 molecules cm^{-3} $ncps^{-1}$ to semi-quantify the concentrations of OOMs, which is widely used in previous studies (Ehn et al., 2014; Yan et al., 2021; Yao et al., 2018). Among the low volatility vapors, it had been demonstrated that nitrate ions exhibit highest charging efficiency toward H_2SO_4 (Ehn et al., 2014; Hyttinen et al., 2015, 2018; Riva et al., 2019b). The estimated concentrations of OOMs thus can be considered as the lower limits with an uncertainty of $\pm$50% according to error propagation (Ehn et al., 2014). Positive matrix factorization (PMF) was also performed for the measured species using Source Finder (SoFi, v6.3) based on Igor and run by

the multilinear engine (ME-2) as detailed in SI-S3 and Figure S3-S6 (Canonaco et al., 2013).

3. Results and discussion

3.1 Chemical characteristic of OOMs

In total, we have identified 562 OOMs, which concentrated in the nC range of 5 to 10, taking up 84.6% of total OOMs during the whole campaign (unless otherwise stated, all the reported values hereafter were corresponding to the average of the whole campaign). Possible precursors of $C_{5\text{-}10}$ OOMs include isoprene (C_5), benzene/alkyl benzenes ($C_{6\text{-}10}$), aliphatic VOCs ($C_{5\text{-}10}$) and monoterpene (C_{10}) according to previous studies (Bianchi et al., 2019; Nie et al., 2022). $C_{\leqslant 4}$ OOMs only took up a small fraction of 6.7% among total OOMs and were likely a result of the decomposition from OOMs with large carbon numbers as suggested by one of our companion studies (Zhang et al., 2022). The rest 8.7% were $C_{>10}$ OOMs which accounted for a dominating fraction (70%, Figure S7) among the extremely low-volatility organic compounds (ELVOC, $C^* < 3 \times 10^{-5}$ μg m^{-3}) based on a volatility parameterization proposed by Donahue and co-workers (Donahue et al., 2011, 2012; Schervish and Donahue, 2020), and potentially poses larger impacts on SOA formation owing to their lower volatility.

We further classified the detected OOMs into four groups based on the number of N atoms they possessed, including non-nitrogen (0N-) OOMs, 1N-OOMs, 2N-OOMs, and 3N-OOMs. Their average fractional contributions to total OOM concentrations as well as the carbon number (nC) distributions are shown in Figure 1. We found 1N-OOMs dominated the total OOM concentration with an average fraction of 50%, followed by 2N-OOMs (26%), demonstrating the dominance of N-containing OOMs among total OOMs. The 3N-OOMs only took up a small fraction (4%) of total OOMs and the rest 20% was 0N-OOMs.

More interestingly, we found 1N-OOMs prevailed among the OOMs with nC$\leqslant$10, yet 2N-OOMs dominated the $C_{>10}$ OOMs (41.8-84.2%), suggesting the increased importance of multi-step bimolecular oxidation in the formation of 2N-OOMs with nC>10. We also note that the fraction of 2N-OOMs increased stepwise with the increase of nC (Figure 1b) while 3N-OOMs don't exhibit a similar dependence. The potential reason is that, with the increase of nC, on the one hand, more active sites are potentially provided to promote the occurrence of multi-step oxidation, but on the other hand, the potential larger steric effect

can hinder multi-step oxidation. From our observation, these two factors lead an overall positive coupling for 2N-OOMs, but result in a non-monotonic trend for 3N-OOMs. Furthermore, these 2N-OOMs with nC>10 had an average molecular composition of $C_{12.5}H_{22.7}O_{2.1}(NO_3)_2$. Assuming the nitrogen atoms are only associated with nitrate group ($-ONO_2$), the mean double bond equivalent value (DBE) (Nie et al., 2022; Xu et al., 2021) was 1.15 on the carbon skeleton, suggesting its origination from aliphatic compounds, such as alkanes, alkenes, etc. (Gong et al., 2005; Mentel et al., 2015; Wang and Hildebrandt Ruiz, 2018).

We thus further classified the 2N-OOMs to their possible VOC precursors following a recently developed workflow proposed by Nie and co-workers, which is based on the up-to-date understanding of VOC oxidation and molecular characters (*i.e.*, number of different elements, DBE) as well as PMF results (Nie et al., 2022), *i.e.*, aromatics ($2N\text{-}OOM_{Aro}$), aliphatics ($2N\text{-}OOM_{Ali}$), and monoterpene ($2N\text{-}OOM_{MT}$). Note that we group isoprene 2N-OOMs ($2N\text{-}OOM_{Iso}$) into $2N\text{-}OOM_{Ali}$ as well because of the low concentration of isoprene in cold season. As a result, the average fractions of $2N\text{-}OOM_{Aro}$, $2N\text{-}OOM_{Ali}$ and $2N\text{-}OOM_{MT}$ among total 2N-OOMs were 16.0%, 64.2% and 15.3%, respectively (Figure 2), suggesting significant contribution of aliphatic compounds to 2N-OOMs formation. Taken together, the increased fraction of 2N-OOMs with the increase of nC and the dominant fraction of $2N\text{-}OOM_{Ali}$ highlight the significant contribution of high-molecular-weight aliphatic precursors (*i.e.*, intermediate volatility or semi-volatile organic compounds, I/SVOCs) to high-molecular-weight 2N-OOM formation, which were potentially important SOA material. We thus focus our attention on the formation of 2N-OOMs in the following sections.

3.2 2N-OOM formation in PM episodes

To investigate the formation mechanisms and factors that may affect the 2N-OOM formation, one clean day (4^{th}-5^{th} November) and one polluted day (7^{th}-8^{th} November) based on the pollution levels, *i.e.*, $PM_{2.5}$ concentrations, were selected for further analysis. Since OOM formation is directly mediated by photochemistry or nighttime chemistry, the clean and polluted cases were thus split into one clean daytime case (CL_{day}), one clean nighttime case (CL_{night}), one polluted daytime case (PL_{day}) and one polluted

193 nighttime case (PL_{night}). Detailed information on durations, pollution levels, meteorological conditions
194 and 2N-OOM concentrations during these four cases were summarized in Table 1.
195 During the whole campaign, the concentrations of 2N-OOMs ranged from 1.1 × 10^6 to 42.0 × 10^6
196 molecule cm^{-3} as shown in Figure 2. We found the concentrations of 2N-OOMs in the polluted cases were
197 1.7-2.7 times higher than those in clean cases. Table 1 further indicates that the absolute abundances of
198 almost 2N-OOM classes were higher during the polluted cases as compared to clean case no matter in the
199 daytime or nighttime except for the daytime $2N\text{-}OOM_{Aro}$. Specifically, $2N\text{-}OOM_{Ali}$ occupied the largest
200 fractions, which were even higher in polluted cases (66-66%) than those in clean cases (56-61%, Figure
201 2). Especially for the $2N\text{-}OOM_{Ali}$ with nC>10, its concentration in polluted cases increased by a factor of
202 2.3-4.8 compared to the clean cases (Figure 3). From PMF analysis, we also identified a factor
203 characterized by a series of $2N\text{-}OOM_{Ali}$ (*i.e.*, $C_nH_{2n-2}O_8N_2$, n=5-11) as the fingerprint molecules (Table
204 S1). This factor tracks the $PM_{2.5}$ concentration well especially during PM episodes (Figure S8), likely due
205 to the availability of adequate aliphatic precursors during pollution episode. Furthermore, $2N\text{-}OOM_{Ali}$
206 with nC>10 presented both higher concentrations and fractions during daytime than nighttime cases
207 (Figure 3), suggesting that the photochemical formation of $2N\text{-}OOM_{Ali}$ prevailed compared to nighttime
208 formation. To compare CL_{night} and PL_{night}, it was also found that the pollution case would lead enhanced
209 importance of nighttime formation pathways of $2N\text{-}OOM_{Ali}$ with nC>10.
210 We note that the fraction of $2N\text{-}OOM_{Ali}$ increased during CL_{night} primarily due to the more evident
211 decrease of $2N\text{-}OOM_{Aro}$ (Table 1), whose formation is dominated by photochemistry. On the other hand,
212 the decrease of $2N\text{-}OOM_{Aro}$ concentrations at PL_{night} was not as obvious as those on CL_{night}. Due to the
213 significant increase of $2N\text{-}OOM_{Ali}$ concentration, the fraction of $2N\text{-}OOM_{Aro}$ decreased in pollution cases,
214 but their absolute concentrations only had few changes in the daytime. $2N\text{-}OOM_{MT}$ showed significant
215 higher concentrations but similar fractions in polluted cases. On the other hand, equivalent or even slightly
216 higher concentrations during nighttime than those in daytime suggest the comparable importance of
217 nighttime chemistry in $2N\text{-}OOM_{MT}$ formation in contrast to $2N\text{-}OOM_{Ali}$ and $2N\text{-}OOM_{Aro}$, which will be
218 discussed in later sections.

To summarize, the absolute concentrations of 2N-OOM were greatly affected by the pollution level for the most cases. Both the concentrations and fractions of 2N-OOM_{Ali} were significantly promoted by pollution condition, whereas the 2N-OOM_{Aro} were predominantly affected by photochemical production, whose formation was less sensitive to pollution levels compared to 2N-OOM_{Ali} in the daytime. In contrast, the absolute concentrations of 2N-OOM_{MT} were also significantly influenced by pollution levels but seem not solely/almost depend on daytime/nighttime formation pathway. In addition, we note that both daytime photochemistry and nighttime chemistry had profound effects on 2N-OOMs formation under different pollution levels, presumably depending on availability of the precursors as well as the oxidants. We thus focus our attention on the formation of 2N-OOMs during daytime versus nighttime in the following sections.

3.3 Daytime vs. nighttime formation of 2N-OOMs

We thus investigate the effects of photochemistry and nighttime chemistry on the formation of individual 2N-OOMs. While the former is dominated by OH radical oxidation, the latter involves NO_3 radical oxidation as well as reactions with ozone or other oxidants, *e.g.*, halogen. Herein, we use solar radiation as a proxy of photochemical reactivity, and the concentrations of NO_3 radical were estimated assuming that NO_3, NO_2 and N_2O_5 were under fast equilibration in troposphere (Brown and Stutz, 2012). The correlation coefficients (Spearman type) between individual 2N-OOM molecules and solar radiation ($R_{2N\text{-}OOMs\text{-}solar}$) or NO_3 radical ($R_{2N\text{-}OOMs\text{-}NO3}$) derived from different precursors during the whole campaign were shown in Figure 4a. It should be noted that the concentrations of 2N-OOMs and NO_3 radicals were scaled with the boundary layer height before calculating the correlation coefficients here and below for correcting the effects of meteorological dilution.

Both 2N-OOM_{Aro} and 2N-OOM_{Ali} showed stronger correlations with solar radiation over NO_3 radicals, indicating their association with daytime photochemistry since benzene/alkyl benzenes and aliphatic VOCs rapidly react with OH radicals compared to other oxidants, such as NO_3 radicals. This is also supported by the observation that both 2N-OOM_{Aro} and 2N-OOM_{Ali} peaked during noontime (12:00-14:00) as shown in Figure 4b. Similarly, the PMF analysis also distinguished two daytime factors. The

daytime factor-1 peaked at around 12:00-14:00 (Table S1) and highly correlated with solar radiation (R=0.57). The fingerprint-molecules of daytime factor-1 are $C_nH_{2n-4}O_{10}N_2$ (n=8-10) with average DBE values of 2 on the carbon skeleton, suggesting the dominance of 2N-OOMs likely formed from aromatic precursors. Since each step of OH oxidation of aromatics followed by RO_2+NO_x termination would increase the nH by one, this factor is likely dominated by 2N-OOMs formed from two steps of OH-initiated oxidation from alkylbenzenes given the carbon numbers ranged from 8 to 10.

The key fingerprint molecule of daytime factor-2 is $C_nH_{2n}O_8N_2$ (n=4-5) (accounting for 30.8% in the factor profile), followed by $C_nH_{2n-2}O_8N_2$ (n=5-6) (accounting for 9.7% in the factor profile), which is likely a result of the decomposition from 2N-OOM_{Ali} with large carbon numbers, according to their DBE values of 0-1 on the carbon skeleton. This aliphatic factor presented even higher correlation with solar radiation (R=0.65), peaking at around 12:00-14:00. Strong daytime peaks together with the good correlations with irradiation suggest the dominance of photochemical oxidation in the formation of 2N-OOM_{Ali}. For 2N-OOM_{Ali}, although it showed strong daytime peak, weak nighttime peak was still observed. This indicates that although daytime formation of 2N-OOM_{Ali} prevails, their nighttime formation still existed. For example, we have obtained a nighttime factor from PMF analysis (nighttime factor-2), whose fingerprint molecules are $C_5H_8O_9N_2$ and $C_nH_{2n}O_7N_2$ (n=5-8). $C_5H_8O_9N_2$ was likely originated from isoprene and $C_nH_{2n}O_7N_2$ were likely from anthropogenic aliphatic precursors.

Nighttime chemistry plays a more important role in the formation of 2N-OOM_{MT}. This is further supported by the slightly stronger correlation between 2N-OOM_{MT} and NO_3 radicals than solar radiation. For some specific 2N-OOM_{MT} species, the formation is likely a result of NO_3 radical initiated oxidation. As shown in Figure 5, we have identified a series of 2N-OOM_{MT} molecules with molecular composition of $C_{10}H_{16}O_{7,9,11}N_2$, which showed strong positive correlations with NO_3 radical. The occurrence of propagation reaction from RO_2 to RO was critical to the formation of odd oxygen as proposed in previous chamber studies (Boyd et al., 2015; Claflin and Ziemann, 2018). Furthermore, under the nighttime conditions observed in urban Shanghai (Table 1), it is estimated that monoterpenes primarily react with NO_3, and the fate of nighttime RO_2s is dominated by NO, which is clear different from rural

environment where NO levels likely drop to near zero after sunset (Romer et al., 2016) and RO_2s are likely terminated by NO_3-RO_2 cross-reactions (Bates et al., 2022). Therefore, formation of $C_{10}H_{16}O_{7,9,11}N_2$ likely started with the reaction of monoterpene with NO_3 radicals forming a NO_3-$C_{10}H_{16}$ alkyl radical, followed by the formation of organic peroxy radical (RO_2) upon addition of O_2. The RO_2 is then converted to an alkoxy radical (RO) upon reaction with NO. The autoxidation process would then start and stepwise introduce O_2 into the molecule, forming a series of more oxygenated RO_2 radicals, *i.e.*, NO_3-$C_{10}H_{16}(O)(OO)_n$. The NO termination reaction of these RO_2 radicals would finally result in ONs with chemical composition of NO_3-$C_{10}H_{16}(O)(OO)_nO(NO)O$ (n=0, 1, 2).

On the other hand, the reaction rate between monoterpenes (i.e., alpha-pinene, beta-pinene and limonene) and NO_3 are about 60,000-140,000 times faster than that between monoterpenes and O_3 at 293K (MCMv3.1), but the averaged nighttime concentrations of O_3 (22.8 ppb) was only about 18,000 times higher than that of NO_3 (1.3 ppt). Therefore, NO_3-initiated oxidation process posed significant impacts on 2N-OOM_{MT} formation during nighttime. The 2N-OOM_{MT} resulted from NO_3 oxidation is also resolved as a nighttime factor (nighttime factor-1) from PMF analysis, which tracked the NO_3 concentrations well (Figure S9, R=0.46) and peaked at around 19:00-23:00. Fingerprint molecule of nighttime factor-1 was mainly including $C_{10}H_{16}O_9N_2$ and $C_{10}H_{16}O_8N_2$, which is generated from NO_3-initiated oxidation followed by NO termination and this process will not change the nH of the parent monoterpene molecule.

3.4 Oxygenation level of 2N-OOMs

We then calculated the average effective oxygen number (nO_{eff} = nO - 2nN) of 2N-OOMs, which is used to indicate the oxidation state of carbon by excluding the oxygen atoms bonded with nitrogen atoms. Note that calculation of nO_{eff} assumes that the nitrogen atoms are only associated with nitrate group (-ONO_2), which is reasonable after excluding nitrophenol peaks. The average nO_{eff} of 2N-OOMs from different precursors in CL_{day}, CL_{night}, PL_{day} and PL_{night} were shown in Figure 6 and summarized in Table S2. 2N-OOM_{Aro} had the highest nO_{eff} (4.8-5.6), followed by 2N-OOM_{MT} (4.5-4.9) and 2N-OOM_{Ali} were of lowest nO_{eff} (3.9-4.0). Difference in the oxygenation level of different types of OOMs can be attributed to the difference in oxidation mechanisms of the initiation reactions. For example, the OH-initiated

297 oxidation of alkanes, aromatics and monoterpene/alkenes would form a $C_xH_yO_2$ radical, $C_xH_yO_5$ radical
298 and $C_xH_yO_3$ radical, respectively, incorporating different number of oxygen atoms into the original
299 precursor molecules at the first step of oxidation (MCMv3.1). On the other hand, during the multiple-step
300 oxidation in daytime, aromatics could still provide more C=C bonds than other precursors after the initial
301 step which is plausibly capable to further react with OH, O_3 and others oxidants.

302 Furthermore, we also found that regardless of the pollution level, the nO_{eff} was considerably higher
303 in daytime cases than that in nighttime cases particularly for 2N-OOM_{Aro} and 2N-OOM_{MT}, suggesting a
304 profound effects of photochemistry on the formation of highly oxygenated 2N-OOMs. This is likely
305 because of the high NO_x concentrations during the nighttime (Table 1), which could efficiently suppress
306 the RO_2 radicals from autoxidation reactions forming overall less oxygenated OOM molecules. The effect
307 of NO_x on oxygenation levels would be discussed in a subsequent paragraph. The average nO_{eff} of 2N-
308 OOM_{Ali} in four sub-periods were similar without significant daytime and nighttime difference, ranging
309 from 3.9-4.0. This could be partly explained by the fact that reactions with oxidants such as OH and
310 halogen radicals will similarly result in the addition of oxygen atoms by two for alkanes during the first
311 step of oxidation. Thus, the oxygenation levels of 2N-OOM_{Ali} were supposed to be insensitive to the
312 oxidants in daytime or nighttime.

313 It is known that NO is also critical in determining the fate of RO_2 radical during the oxidation,
314 forming RO radicals or organonitrates. Formation of RO radicals and organonitrates will have opposite
315 effects on the oxidation state of the termination products since the former will significantly increase the
316 oxygenation state of carbon through initiating propagation reactions before termination. We thus explore
317 the effects of NO as well as the total NO_x concentrations on the average oxygenation levels of 2N-OOMs
318 from different precursors during the whole campaign (Figure 7). Consistent with previous studies in
319 polluted urban environment (Qiao et al., 2021; Yan et al., 2021), the detected 2N-OOMs were also of low
320 oxygenation with nO_{eff} of 3.9-5.4 (25-75% percentile) compared to those measured in forest or in
321 laboratory studies (Berndt et al., 2016; Ehn et al., 2014; Jokinen et al., 2014; Rissanen et al., 2014; Yan et
322 al., 2016). nO_{eff} of 2N-OOM_{Aro} and 2N-OOM_{MT} increased with the decrease of NO/NO_x concentrations.

This is likely due to the prevailing of NO termination reactions because the maximum autoxidation rate constant of alkylbenzenes with long-chain substituents (e.g., isopropyl-benzene, ethyl-benzene) and monoterpene are comparable to the bimolecular reaction rate between RO_2 and NO (Bianchi et al., 2019). The oxygenation levels of 2N-OOM_{Ali} appears to be insensitive to the pollution levels and NO/NO_x concentrations, which should be further investigated in future studies.

4 Conclusion

We report the unambiguous identification of 2N-OOMs as well as other OOMs using an ultra-high-resolution orbitrap coupled with a nitrate inlet. We found that OOMs distributed in a wide range of carbon numbers (nC = 4 - 16), among which the 2N-OOMs occupied a considerable fraction (26%) of the total observed OOMs. During the whole campaign, the 2N-OOM concentrations ranged from 1.1 × 10^6 to 42.0 × 10^6 molecule cm^{-3} and concentrated in the nC range of 5 to 10 with high molecular weight (m/z > 350 Th), suggesting their low volatilities and thus potentially high contribution to local SOA formation.

Aliphatic, aromatics, and monoterpenes were plausible precursors of 2N-OOMs with a fraction of 64.2%, 16% and 15.4%, respectively. The absolute concentrations of 2N-OOMs were greatly affected by the pollution level for the most cases. The 2N-OOM_{Ali} was found to be the most abundant 2N-OOMs and its fraction even increased in the polluted day with enhanced proportion of ones with nC>10, probably due to the high concentrations of aliphatic precursors accompanied with PM episodes. Significant contribution of long-chain aliphatic compounds (nC > 10) to 2N-OOM formation is also supported by the observation that 2N-OOM fraction increased with the increase of nC and they are of low DBE values, likely through multistep bimolecular oxidation. 2N-OOM_{Ali} and 2N-OOM_{Aro} mainly peaked in daytime and showed stronger correlations with solar radiation over NO_3 radicals, indicating their association with daytime photochemistry since benzene/alkyl benzenes and aliphatic hydrocarbons rapidly react with OH radicals compared with other oxidants, such as NO_3 radicals. In contrast, 2N-OOM_{MT} prevailed both in daytime and nighttime, some specific 2N-OOM_{MT} species showed strong positive correlations with NO_3 radical and were likely a result of NO_3 radical initiated oxidation, suggesting the comparable importance of nighttime NO_3 chemistry in 2N-OOM_{MT} formation. In terms of oxygenation levels, we found that 2N-

OOM_{Aro} had highest averaged nO_{eff} followed by 2N-OOM_{MT}. Daytime photochemistry and low NO_x concentrations had profound effects on the formation of more oxygenated 2N-OOMs. 2N-OOM_{Ali} had the lowest nO_{eff} and had negligible changes under different pollution levels. These results demonstrate the preference of 2N-OOM formation and the influencing factors in a Chinese megacity involving various VOC precursors (biogenic VOCs such as monoterpene and anthropogenic VOCs such as aromatics, aliphatic hydrocarbons) and various atmospheric oxidants (such as OH radical and NO_3 radicals), and highlight the influence of PM episode.

Code/Data availability

Data presented in this paper are available upon request to the corresponding author.

Author contributions

CH designed this study. YL, YM, DDH, SL, SJ, and YG conducted the field campaign. YL analyzed data with contributions from CH and all the other co-authors. YL wrote the manuscript with contributions from all the other co-authors.

Competing interests

The authors declare that they have no conflict of interest.

Acknowledgement

This study was financially supported by the Funded by the National Key R&D Program of China (2022YFC3700205), and China Postdoctoral Science Foundation (2022T150427).

Reference

Atkinson, R. and Arey, J.: Atmospheric Degradation of Volatile Organic Compounds, Chem. Rev., 103(3), 4605–4638, doi:10.1021/cr0206420, 2003.

Bates, K. H., Burke, G. J. P., Cope, J. D. and Nguyen, T. B.: Secondary organic aerosol and organic nitrogen yields from the nitrate radical (NO3) oxidation of alpha-pinene from various RO2 fates, Atmos. Chem. Phys., 22(2), 1467–1482, doi:10.5194/acp-22-1467-2022, 2022.

Berndt, T., Richters, S., Jokinen, T., Hyttinen, N., Kurtén, T., Otkjær, R. V., Kjaergaard, H. G., Stratmann, F., Herrmann, H., Sipilä, M., Kulmala, M. and Ehn, M.: Hydroxyl radical-induced formation of

highly oxidized organic compounds, Nat. Commun., 7(13677), doi:10.1038/ncomms13677, 2016.

Berndt, T., Scholz, W., Mentler, B., Fischer, L., Herrmann, H., Kulmala, M. and Hansel, A.: Accretion Product Formation from Self- and Cross-Reactions of RO2 Radicals in the Atmosphere, Angew. Chemie - Int. Ed., 57(14), 3820–3824, doi:10.1002/anie.201710989, 2018.

Bianchi, F., Kurtén, T., Riva, M., Mohr, C., Rissanen, M. P., Roldin, P., Berndt, T., Crounse, J. D., Wennberg, P. O., Mentel, T. F., Wildt, J., Junninen, H., Jokinen, T., Kulmala, M., Worsnop, D. R., Thornton, J. A., Donahue, N., Kjaergaard, H. G. and Ehn, M.: Highly Oxygenated Molecules (HOM) from Gas-Phase Autoxidation Involving Organic Peroxy Radicals: A Key Contributor to Atmospheric Aerosol, Chem. Rev., 119, 3472–3509, doi:10.1021/acs.chemrev.8b00395, 2019.

Boyd, C. M., Sanchez, J., Xu, L., Eugene, A. J., Nah, T., Tuet, W. Y., Guzman, M. I. and Ng, N. L.: Secondary organic aerosol formation from the β-pinene+NO3 system: Effect of humidity and peroxy radical fate, Atmos. Chem. Phys., 15(13), 7497–7522, doi:10.5194/acp-15-7497-2015, 2015.

Brown, S. S. and Stutz, J.: Nighttime radical observations and chemistry, Chem. Soc. Rev., 41, 6405–6447, doi:10.1039/c2cs35181a, 2012.

Cai, R., Li, Y., Clément, Y., Li, D., Dubois, C., Fabre, M., Besson, L., Perrier, S., George, C., Ehn, M., Huang, C., Yi, P., Ma, Y. and Riva, M.: Orbitool: A software tool for analyzing online Orbitrap mass spectrometry data, Atmos. Meas. Tech., 14, 2377–2387, doi:10.5194/amt-2020-267, 2020.

Canonaco, F., Crippa, M., Slowik, J. G., Baltensperger, U. and Prévôt, A. S. H. H.: SoFi, an IGOR-based interface for the efficient use of the generalized multilinear engine (ME-2) for the source apportionment: ME-2 application to aerosol mass spectrometer data, Atmos. Meas. Tech., 6(12), 3649–3661, doi:10.5194/amt-6-3649-2013, 2013.

Claflin, M. S. and Ziemann, P. J.: Identification and Quantitation of Aerosol Products of the Reaction of β-Pinene with NO3 Radicals and Implications for Gas- and Particle-Phase Reaction Mechanisms, J. Phys. Chem. A, 122(14), 3640–3652, doi:10.1021/acs.jpca.8b00692, 2018.

Ditto, J. C., Joo, T., Slade, J. H., Shepson, P. B., Ng, N. L. and Gentner, D. R.: Nontargeted Tandem Mass Spectrometry Analysis Reveals Diversity and Variability in Aerosol Functional Groups across

Multiple Sites, Seasons, and Times of Day, Environ. Sci. Technol. Lett., 7(2), 60–69, doi:10.1021/acs.estlett.9b00702, 2020.

Donahue, N. M., Robinson, A. L. and Pandis, S. N.: Atmospheric organic particulate matter: From smoke to secondary organic aerosol, Atmos. Environ., 43(1), 94–106, doi:10.1016/j.atmosenv.2008.09.055, 2009.

Donahue, N. M., Epstein, S. A., Pandis, S. N. and Robinson, A. L.: A two-dimensional volatility basis set: 1. organic-aerosol mixing thermodynamics, Atmos. Chem. Phys., 11(7), 3303–3318, doi:10.5194/acp-11-3303-2011, 2011.

Donahue, N. M., Kroll, J. H., Pandis, S. N. and Robinson, A. L.: A two-dimensional volatility basis set-Part 2: Diagnostics of organic-aerosol evolution, Atmos. Chem. Phys., 12(2), 615–634, doi:10.5194/acp-12-615-2012, 2012.

Ehn, M., Thornton, J. A., Kleist, E., Sipilä, M., Junninen, H., Pullinen, I., Springer, M., Rubach, F., Tillmann, R., Lee, B., Lopez-Hilfiker, F., Andres, S., Acir, I.-H. H., Rissanen, M., Jokinen, T., Schobesberger, S., Kangasluoma, J., Kontkanen, J., Nieminen, T., Kurtén, T., Nielsen, L. B., Jørgensen, S., Kjaergaard, H. G., Canagaratna, M., Maso, M. D., Berndt, T., Petäjä, T., Wahner, A., Kerminen, V.-M. M., Kulmala, M., Worsnop, D. R., Wildt, J. and Mentel, T. F.: A large source of low-volatility secondary organic aerosol, Nature, 506(7489), 476–479, doi:10.1038/nature13032, 2014.

Garmash, O., Rissanen, M. P., Pullinen, I., Schmitt, S., Kausiala, O., Tillmann, R., Zhao, D., Percival, C., Bannan, T. J., Priestley, M., Hallquist, A. M., Kleist, E., Kiendler-Scharr, A., Hallquist, M., Berndt, T., McFiggans, G., Wildt, J., Mentel, T. F. and Ehn, M.: Multi-generation OH oxidation as a source for highly oxygenated organic molecules from aromatics, Atmos. Chem. Phys., 20(1), 515–537, doi:10.5194/acp-20-515-2020, 2020.

Gong, H., Matsunaga, A. and Ziemann, P. J.: Products and mechanism of secondary organic aerosol formation from reactions of linear alkenes with NO3 Radicals, J. Phys. Chem. A, 109(19), 4312–4324, doi:10.1021/jp058024l, 2005.

Hallquist, M., Wenger, J. C., Baltensperger, U., Rudich, Y., Simpson, D., Claeys, M., Dommen, J., Donahue, N. M., George, C., Goldstein, A. H., Hamilton, J. F., Herrmann, H., Hoffmann, T., Iinuma, Y., Jang, M., Jenkin, M. E., Jimenez, J. L., Kiendler-Scharr, A., Maenhaut, W., McFiggans, G., Mentel, T. F., Monod, A., Prévôt, A. S. H., Seinfeld, J. H., Surratt, J. D., Szmigielski, R. and Wildt, J.: The formation, properties and impact of secondary organic aerosol: Current and emerging issues, Atmos. Chem. Phys., 9(14), 5155–5236, doi:10.5194/acp-9-5155-2009, 2009.

Heinritzi, M., Simon, M., Steiner, G., Wagner, A. C., K??rten, A., Hansel, A. and Curtius, J.: Characterization of the mass-dependent transmission efficiency of a CIMS, Atmos. Meas. Tech., 9(4), 1449–1460, doi:10.5194/amt-9-1449-2016, 2016.

Hyttinen, N., Kupiainen-Määtta, O., Rissanen, M. P., Muuronen, M., Ehn, M. and Kurtén, T.: Modeling the Charging of Highly Oxidized Cyclohexene Ozonolysis Products Using Nitrate-Based Chemical Ionization, J. Phys. Chem. A, 119(24), 6339–6345, doi:10.1021/acs.jpca.5b01818, 2015.

Hyttinen, N., Otkjær, R. V., Iyer, S., Kjaergaard, H. G., Rissanen, M. P., Wennberg, P. O. and Kurtén, T.: Computational Comparison of Different Reagent Ions in the Chemical Ionization of Oxidized Multifunctional Compounds, J. Phys. Chem. A, 122(1), 269–279, doi:10.1021/acs.jpca.7b10015, 2018.

Jimenez, J. L., Canagaratna, M. R., Donahue, N. M., Prevot, A. S. H. H., Zhang, Q., Kroll, J. H., DeCarlo, P. F., Allan, J. D., Coe, H., Ng, N. L., Aiken, A. C., Docherty, K. S., Ulbrich, I. M., Grieshop, A. P., Robinson, A. L., Duplissy, J., Smith, J. D., Wilson, K. R., Lanz, V. A., Hueglin, C., Sun, Y. L., Tian, J., Laaksonen, A., Raatikainen, T., Rautiainen, J., Vaattovaara, P., Ehn, M., Kulmala, M., Tomlinson, J. M., Collins, D. R., Cubison, M. J., Dunlea, J., Huffman, J. A., Onasch, T. B., Alfarra, M. R., Williams, P. I., Bower, K., Kondo, Y., Schneider, J., Drewnick, F., Borrmann, S., Weimer, S., Demerjian, K., Salcedo, D., Cottrell, L., Griffin, R., Takami, A., Miyoshi, T., Hatakeyama, S., Shimono, A., Sun, J. Y., Zhang, Y. M., Dzepina, K., Kimmel, J. R., Sueper, D., Jayne, J. T., Herndon, S. C., Trimborn, A. M., Williams, L. R., Wood, E. C., Middlebrook, A. M., Kolb, C. E., Baltensperger, U., Worsnop, D. R., Dunlea, E. J., Huffman, J. A., Onasch, T. B., Alfarra, M. R., Williams, P. I.,

Bower, K., Kondo, Y., Schneider, J., Drewnick, F., Borrmann, S., Weimer, S., Demerjian, K., Salcedo, D., Cottrell, L., Griffin, R., Takami, A., Miyoshi, T., Hatakeyama, S., Shimono, A., Sun, J. Y., Zhang, Y. M., Dzepina, K., Kimmel, J. R., Sueper, D., Jayne, J. T., Herndon, S. C., Trimborn, A. M., Williams, L. R., Wood, E. C., Middlebrook, A. M., Kolb, C. E., Baltensperger, U. and Worsnop, D. R.: Evolution of Organic Aerosols in the Atmosphere, Science (80-.)., 326(5959), 1525–1529, doi:10.1126/science.1180353, 2009.

Jokinen, T., Sipilä, M., Richters, S., Kerminen, V. M., Paasonen, P., Stratmann, F., Worsnop, D., Kulmala, M., Ehn, M., Herrmann, H. and Berndt, T.: Rapid autoxidation forms highly oxidized RO2 radicals in the atmosphere, Angew. Chemie Int. Ed., 53, 14596–14600, doi:10.1002/anie.201408566, 2014.

Jokinen, T., Berndt, T., Makkonen, R., Kerminen, V.-M., Junninen, H., Paasonen, P., Stratmann, F., Herrmann, H., Guenther, A. B., Worsnop, D. R., Kulmala, M., Ehn, M. and Sipilä, M.: Production of extremely low volatile organic compounds from biogenic emissions: Measured yields and atmospheric implications, Proc. Natl. Acad. Sci., 112(23), 7123–7128, doi:10.1073/pnas.1423977112, 2015.

Junninen, H., Ehn, M., Petäjä, Luosujärvi, L., Kotiaho, T., Kostiainen, R., Rohner, U., Gonin, M., Fuhrer, K., Kulmala, M. and Worsnop, D. R.: A high-resolution mass spectrometer to measure atmospheric ion composition, Atmos. Meas. Tech., 3(4), 1039–1053, doi:10.5194/amt-3-1039-2010, 2010.

Kenagy, H. S., Present, P. S. R., Wooldridge, P. J., Nault, B. A., Campuzano-jost, P., Day, D. A., Jimenez, J. L., Zare, A., Pye, H. O. T., Yu, J., Song, C. H., Blake, D. R., Woo, J., Kim, Y. and Cohen, R. C.: Contribution of Organic Nitrates to Organic Aerosol over South Korea during KORUS-AQ, Environ. Sci. Technol., 55, 16326−16338, doi:10.1021/acs.est.1c05521, 2021.

Kiendler-Scharr, A., Mensah, A. A., Friese, E., Topping, D., Nemitz, E., Prevot, A. S. H., Äijälä, M., Allan, J., Canonaco, F., Canagaratna, M., Carbone, S., Crippa, M., Dall Osto, M., Day, D. A., De Carlo, P., Di Marco, C. F., Elbern, H., Eriksson, A., Freney, E., Hao, L., Herrmann, H., Hildebrandt, L., Hillamo, R., Jimenez, J. L., Laaksonen, A., McFiggans, G., Mohr, C., O'Dowd, C., Otjes, R., Ovadnevaite, J., Pandis, S. N., Poulain, L., Schlag, P., Sellegri, K., Swietlicki, E., Tiitta, P.,

Vermeulen, A., Wahner, A., Worsnop, D. and Wu, H. C.: Ubiquity of organic nitrates from nighttime chemistry in the European submicron aerosol, Geophys. Res. Lett., 43(14), 7735–7744, doi:10.1002/2016GL069239, 2016.

Lee, B. H., Mohr, C., Lopez-Hilfiker, F. D., Lutz, A., Hallquist, M., Lee, L., Romer, P., Cohen, R. C., Iyer, S., Kurtén, T., Hu, W., Day, D. A., Campuzano-Jost, P., Jimenez, J. L., Xu, L., Ng, N. L., Guo, H., Weber, R. J., Wild, R. J., Brown, S. S., Koss, A., De Gouw, J., Olson, K., Goldstein, A. H., Seco, R., Kim, S., McAvey, K., Shepson, P. B., Starn, T., Baumann, K., Edgerton, E. S., Liu, J., Shilling, J. E., Miller, D. O., Brune, W., Schobesberger, S., D'Ambro, E. L. and Thornton, J. A.: Highly functionalized organic nitrates in the southeast United States: Contribution to secondary organic aerosol and reactive nitrogen budgets, Proc. Natl. Acad. Sci. U. S. A., 113(6), 1516–1521, doi:10.1073/pnas.1508108113, 2016.

Lee Ng, N., Brown, S. S., Archibald, A. T., Atlas, E., Cohen, R. C., Crowley, J. N., Day, D. A., Donahue, N. M., Fry, J. L., Fuchs, H., Griffin, R. J., Guzman, M. I., Herrmann, H., Hodzic, A., Iinuma, Y., Kiendler-Scharr, A., Lee, B. H., Luecken, D. J., Mao, J., McLaren, R., Mutzel, A., Osthoff, H. D., Ouyang, B., Picquet-Varrault, B., Platt, U., Pye, H. O. T., Rudich, Y., Schwantes, R. H., Shiraiwa, M., Stutz, J., Thornton, J. A., Tilgner, A., Williams, B. J. and Zaveri, R. A.: Nitrate radicals and biogenic volatile organic compounds: Oxidation, mechanisms, and organic aerosol, Atmos. Chem. Phys., 17(3), 2103–2162, doi:10.5194/acp-17-2103-2017, 2017.

Liebmann, J., Sobanski, N., Schuladen, J., Karu, E., Hellén, H., Hakola, H., Zha, Q., Ehn, M., Riva, M., Williams, J., Fischer, H., Lelieveld, J. and Crowley, J. N.: Alkyl nitrates in the boreal forest: Formation via the NO3, OH and O3 induced oxidation of BVOCs and ambient lifetimes, Atmos. Chem. Phys. Discuss., (3), 1–23, doi:10.5194/acp-2019-463, 2019.

Lin, C., Huang, R. J., Duan, J., Zhong, H. and Xu, W.: Primary and Secondary Organic Nitrate in Northwest China: A Case Study, Environ. Sci. Technol. Lett., 8(11), 947–953, doi:10.1021/acs.estlett.1c00692, 2021.

Mentel, T. F., Springer, M., Ehn, M., Kleist, E., Pullinen, I., Kurtén, T., Rissanen, M., Wahner, A. and

Wildt, J.: Formation of highly oxidized multifunctional compounds: autoxidation of peroxy radicals formed in the ozonolysis of alkenes-deduced from structure–product relationships, Atmos. Chem. Phys. Discuss., 15(2), 2791–2851, doi:10.5194/acpd-15-2791-2015, 2015.

Nie, W., Yan, C., Huang, D. D., Wang, Z., Liu, Y., Qiao, X., Guo, Y., Tian, L., Zheng, P., Xu, Z., Li, Y., Xu, Z., Qi, X., Sun, P., Wang, J., Zheng, F., Li, X., Yin, R., Dallenbach, K. R., Bianchi, F., Petäjä, T., Zhang, Y., Wang, M., Schervish, M., Wang, S., Qiao, L., Wang, Q., Zhou, M., Wang, H., Yu, C., Yao, D., Guo, H., Ye, P., Lee, S., Li, Y. J., Liu, Y., Chi, X., Kerminen, V.-M., Ehn, M., Donahue, N. M., Wang, T., Huang, C., Kulmala, M., Worsnop, D., Jiang, J. and Ding, A.: Secondary organic aerosol formed by condensing anthropogenic vapours over China's megacities, Nat. Geosci., 15, 255–261, doi:10.1038/s41561-022-00922-5, 2022.

Pye, H. O. T., D'Ambro, E. L., Lee, B. H., Schobesberger, S., Takeuchi, M., Zhao, Y., Lopez-Hilfiker, F., Liu, J., Shilling, J. E., Xing, J., Mathur, R., Middlebrook, A. M., Liao, J., Welti, A., Graus, M., Warneke, C., de Gouw, J. A., Holloway, J. S., Ryerson, T. B., Pollack, I. B. and Thornton, J. A.: Anthropogenic enhancements to production of highly oxygenated molecules from autoxidation, Proc. Natl. Acad. Sci. U. S. A., 116(14), 6641–6646, doi:10.1073/pnas.1810774116, 2019.

Qiao, X., Yan, C., Li, X., Guo, Y., Yin, R., Deng, C., Li, C., Nie, W., Wang, M., Cai, R., Huang, D., Wang, Z., Yao, L., Worsnop, D. R., Bianchi, F., Liu, Y., Donahue, N. M., Kulmala, M. and Jiang, J.: Contribution of Atmospheric Oxygenated Organic Compounds to Particle Growth in an Urban Environment, Environ. Sci. Technol., doi:10.1021/acs.est.1c02095, 2021.

Rissanen, M. P., Kurtén, T., Sipilä, M., Thornton, J. A., Kangasluoma, J., Sarnela, N., Junninen, H., Jørgensen, S., Schallhart, S., Kajos, M. K., Taipale, R., Springer, M., Mentel, T. F., Ruuskanen, T., Petäjä, T., Worsnop, D. R., Kjaergaard, H. G. and Ehn, M.: The formation of highly oxidized multifunctional products in the ozonolysis of cyclohexene, J. Am. Chem. Soc., 136(44), 15596–15606, doi:10.1021/ja507146s, 2014.

Riva, M.: Multiphase Chemistry of Highly Oxidized Molecules: The Case of Organic Hydroperoxides, Chem, 1(4), 526–528, doi:10.1016/j.chempr.2016.09.015, 2016.

Riva, M., Ehn, M., Li, D., Tomaz, S., Bourgain, F., Perrier, S. and George, C.: CI-Orbitrap: An Analytical Instrument to Study Atmospheric Reactive Organic Species, Anal. Chem., 91, 9419–9423, doi:10.1021/acs.analchem.9b02093, 2019a.

Riva, M., Rantala, P., Krechmer, J. E., Peräkylä, O., Zhang, Y., Heikkinen, L., Garmash, O., Yan, C., Kulmala, M., Worsnop, D. and Ehn, M.: Evaluating the performance of five different chemical ionization techniques for detecting gaseous oxygenated organic species, Atmos. Meas. Tech., 12, 2403–2421, doi:10.5194/amt-2018-407, 2019b.

Rollins, A. W., Pusede, S., Wooldridge, P., Min, K. E., Gentner, D. R., Goldstein, A. H., Liu, S., Day, D. A., Russell, L. M., Rubitschun, C. L., Surratt, J. D. and Cohen, R. C.: Gas/particle partitioning of total alkyl nitrates observed with TD-LIF in Bakersfield, J. Geophys. Res. Atmos., 118(12), 6651–6662, doi:10.1002/jgrd.50522, 2013.

Romer, P. S., Duffey, K. C., Wooldridge, P. J., Allen, H. M., Ayres, B. R., Brown, S. S., Brune, W. H., Crounse, J. D., De Gouw, J., Draper, D. C., Feiner, P. A., Fry, J. L., Goldstein, A. H., Koss, A., Misztal, P. K., Nguyen, T. B., Olson, K., Teng, A. P., Wennberg, P. O., Wild, R. J., Zhang, L. and Cohen, R. C.: The lifetime of nitrogen oxides in an isoprene-dominated forest, Atmos. Chem. Phys., 16(12), 7623–7637, doi:10.5194/acp-16-7623-2016, 2016.

Schervish, M. and Donahue, N. M.: Peroxy radical chemistry and the volatility basis set, Atmos. Chem. Phys., 20(2), 1183–1199, doi:10.5194/acp-20-1183-2020, 2020.

Wang, D. S. and Hildebrandt Ruiz, L.: Chlorine-initiated oxidation of n-alkanes under high NOx conditions: Insights into secondary organic aerosol composition and volatility using a FIGAERO-CIMS, Atmos. Chem. Phys. Discuss., (x), 1–26, doi:10.5194/acp-2018-443, 2018.

Wang, Y., Mehra, A., Krechmer, J., Yang, G., Hu, X., Lu, Y., Lambe, A., Canagaratna, M., Chen, J., Worsnop, D., Coe, H. and Wang, L.: Oxygenated products formed from OH-initiated reactions of trimethylbenzene: Autoxidation and accretion, Atmos. Chem. Phys., 20, 9563–9579, doi:10.5194/acp-2020-165, 2020.

Xu, L., Suresh, S., Guo, H., Weber, R. J. and Ng, N. L.: Aerosol characterization over the southeastern

United States using high-resolution aerosol mass spectrometry: Spatial and seasonal variation of aerosol composition and sources with a focus on organic nitrates, Atmos. Chem. Phys., 15(13), 7307–7336, doi:10.5194/acp-15-7307-2015, 2015.

Xu, Z. N., Nie, W., Liu, Y. L., Sun, P., Huang, D. D., Yan, C., Krechmer, J., Ye, P. L., Xu, Z., Qi, X. M., Zhu, C. J., Li, Y. Y., Wang, T. Y., Wang, L., Huang, X., Tang, R. Z., Guo, S., Xiu, G. L., Fu, Q. Y., Worsnop, D., Chi, X. G. and Ding, A. J.: Multifunctional Products of Isoprene Oxidation in Polluted Atmosphere and Their Contribution to SOA, Geophys. Res. Lett., 48(1), 1–10, doi:10.1029/2020GL089276, 2021.

Yan, C., Nie, W., Äijälä, M., Rissanen, M. P., Canagaratna, M. R., Massoli, P., Junninen, H., Jokinen, T., Sarnela, N., Häme, S. A. K., Schobesberger, S., Canonaco, F., Yao, L., Prévôt, A. S. H., Petäjä, T., Kulmala, M., Sipilä, M., Worsnop, D. R. and Ehn, M.: Source characterization of highly oxidized multifunctional compounds in a boreal forest environment using positive matrix factorization, Atmos. Chem. Phys., 16, 12715–12731, doi:10.5194/acp-16-12715-2016, 2016.

Yan, C., Yin, R., Lu, Y., Dada, L., Yang, D., Fu, Y., Kontkanen, J., Deng, C., Garmash, O., Ruan, J., Baalbaki, R., Schervish, M., Cai, R., Bloss, M., Chan, T., Chen, T., Chen, Q., Chen, X., Chen, Y., Chu, B., Dällenbach, K., Foreback, B., He, X., Heikkinen, L., Jokinen, T., Junninen, H., Kangasluoma, J., Kokkonen, T., Kurppa, M., Lehtipalo, K., Li, H., Li, H., Li, X., Liu, Y., Ma, Q., Paasonen, P., Rantala, P., Pileci, R. E., Rusanen, A., Sarnela, N., Simonen, P., Wang, S., Wang, W., Wang, Y., Xue, M., Yang, G., Yao, L., Zhou, Y., Kujansuu, J., Petäjä, T., Nie, W., Ma, Y., Ge, M., He, H., Donahue, N. M., Worsnop, D. R., Veli-Matti Kerminen, Wang, L., Liu, Y., Zheng, J., Kulmala, M., Jiang, J. and Bianchi, F.: The Synergistic Role of Sulfuric Acid, Bases, and Oxidized Organics Governing New-Particle Formation in Beijing, Geophys. Res. Lett., 48, 2020GL091944, doi:10.1029/2020gl091944, 2021.

Yao, L., Garmash, O., Bianchi, F., Zheng, J., Yan, C., Kontkanen, J., Junninen, H., Mazon, S. B., Ehn, M., Paasonen, P., Sipilä, M., Wang, M., Wang, X., Xiao, S., Chen, H., Lu, Y., Zhang, B., Wang, D., Fu, Q., Geng, F., Li, L., Wang, H., Qiao, L., Yang, X., Chen, J., Kerminen, V.-M., Petäjä, T., Worsnop,

583 D. R., Kulmala, M. and Wang, L.: Atmospheric new particle formation from sulfuric acid and amines
584 in a Chinese megacity, Science (80-.)., 361, 278–281, doi:10.1126/science.aao4839, 2018.
585 Ye, C., Yuan, B., Lin, Y., Wang, Z., Hu, W., Li, T., Chen, W., Wu, C., Wang, C., Huang, S., Qi, J., Wang,
586 B., Wang, C., Song, W., Wang, X., Zheng, E., Krechmer, J. E., Ye, P., Zhang, Z., Wang, X., Worsnop,
587 D. R. and Shao, M.: Chemical characterization of oxygenated organic compounds in the gas phase
588 and particle phase using iodide CIMS with FIGAERO in urban air, Atmos. Chem. Phys., 21(11),
589 8455–8478, doi:10.5194/acp-21-8455-2021, 2021.
590 Yu, K., Zhu, Q., Du, K. and Huan, X. F.: Characterization of nighttime formation of particulate organic
591 nitrates based on high-resolution aerosol mass spectrometry in an urban atmosphere in China, Atmos.
592 Chem. Phys., 19(7), 5235–5249, doi:10.5194/acp-19-5235-2019, 2019.
593 Zhang, Y., Li, D., Ma, Y., Dubois, C., Wang, X., Perrier, S., Chen, H., Wang, H., Jing, S., Lu, Y., Lou,
594 S., Yan, C., Nie, W., Chen, J., Huang, C., George, C. and Riva, M.: Field Detection of Highly
595 Oxygenated Organic Molecules in Shanghai by Chemical Ionization–Orbitrap, Environ. Sci.
596 Technol., doi:10.1021/acs.est.1c08346, 2022.
597 Zhao, Y., Thornton, J. A. and Pye, H. O. T.: Quantitative constraints on autoxidation and dimer formation
598 from direct probing of monoterpene-derived peroxy radical chemistry, Proc. Natl. Acad. Sci. U. S.
599 A., 115(48), 12142–12147, doi:10.1073/pnas.1812147115, 2018.
600

Table 1 Summary of the four cases including the meteorological conditions and concentrations of trace gases and 2N-OOMs

Case	Time	$\overline{PM_{2.5}}$ (μg m^{-3})	$\overline{Solar}$ (W m^{-2})	$\overline{T}$ (°C)	$\overline{RH}$ (%)	$\overline{[O_3]}$ (ppb)	$\overline{[NO]}$ (ppb)	$\overline{[NO_2]}$ (ppb)	$\overline{[NO_3]}$ (ppt)	$\overline{[2N-OOM_{Aro}]}$ (×10^6 cm^{-3})	$\overline{[2N-OOM_{Alk}]}$ (×10^6 cm^{-3})	$\overline{[2N-OOM_{MT}]}$ (×10^6 cm^{-3})	$\overline{[2N-OOM_{Total}]}$ (×10^6 cm^{-3})
CL_{day}	Nov. 4th 12:00 - 14:00	7.5	635.6	18.9	35.2	41.9	3.2	8.2	0.1	6.3	11.7	2.3	20.8
CL_{night}	Nov. 4th 23:00 - Nov. 5th 01:00	9.5	2.4	13.0	64.1	8.0	2.9	40.5	0.2	1.3	6.0	2.3	9.8
PL_{day}	Nov. 7th 12:00 - 14:00	44.0	384.5	23.9	30.5	73.9	2.2	20.6	0.3	6.4	23.8	4.3	36.2
PL_{night}	Nov. 7th 23:00 - Nov. 8th 01:00	60.5	2.5	17.8	44.9	27.2	2.1	38.7	6.2	3.1	17.4	5.3	26.5

Figure Captions

Figure 1. (a) Average mass spectrum of the detected OOMs during the whole campaign. The pie chart shows the fractions of OOMs with different number of nitrogen and carbon atoms; (b) The fractions of 0N-OOMs, 1N-OOMs, 2N-OOMs and 3N-OOMs among total OOMs as a function of carbon number (nC).

Figure 2. The timeseries of 2N-OOMs originated from different precursors. Four sub-periods were selected to further investigate the fractional distribution of different type of OOM molecules as shown in the pie chart, including a clean daytime case (12:00 to 14:00 on November 4th, $PM_{2.5}$=7.5 μg m^{-3}, CL_{day}), a clean nighttime case (23:00 on November 4th to 01:00 on November 5th, $PM_{2.5}$=9.5 μg m^{-3}, CL_{night}), a daytime case in a PM episode (12:00 to 14:00 on November 7th, $PM_{2.5}$=44.0 μg m^{-3}, PL_{day}) and a nighttime case in a PM episode (23:00 on November 7th to 01:00 on November 8th, $PM_{2.5}$=60.5 μg m^{-3}, PL_{night}). The sizes of pie charts are scaled to the total concentrations of 2N-OOMs.

Figure 3. The fractions of $2N\text{-}OOM_{Ali}$ with different carbon numbers in the four cases.

Figure 4. (a) Statistical distribution of the correlation coeffients (Spearman type) between 2N-OOMs and solar radiation ($R_{2N\text{-}OOMs\ -\ solar}$) in red and the correlation coeffients between 2N-OOMs and [NO_3] ($R_{2N\text{-}OOMs\ -\ NO3}$) in blue for 2N-OOMs from different precursors. The horizontal lines are the median values, boxes denote the 25th- and 75th- percentile values, and whiskers represent the 10th- and 90th- percentile values. (b) The diel patterns of 2N-OOMs from different precursors.

Figure 5. Scatter plot of $R_{2N\text{-}OOMs\ -\ NO3}$ against $R_{2N\text{-}OOMs\ -\ solar}$ for specific 2N-OOM species.

Figure 6. The nO_{eff} of 2N-OOMs derived from different precursors in the four cases, the error bars represent the standard deviations.

Figure 7. Effective oxygen number (nO_{eff}) of 2N-OOMs as a function of (a) NO concentration and (b) NO_x concentration. The colored squares represent the real measurements. The filled markers indicate the median values in the range as horizontal error bars show, the vertical error bars denote the 25th- and 75th-percentile values.

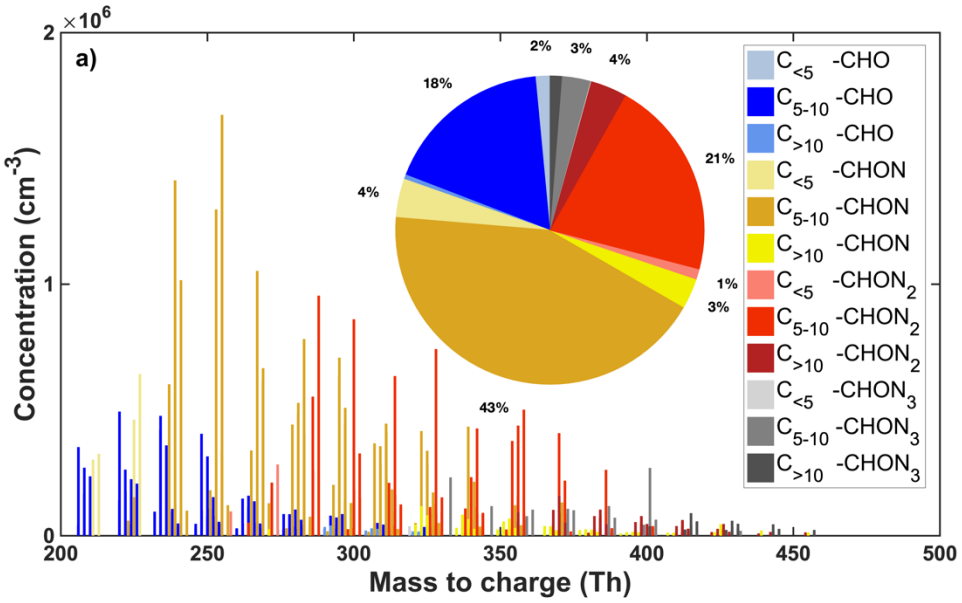

Figure 1a

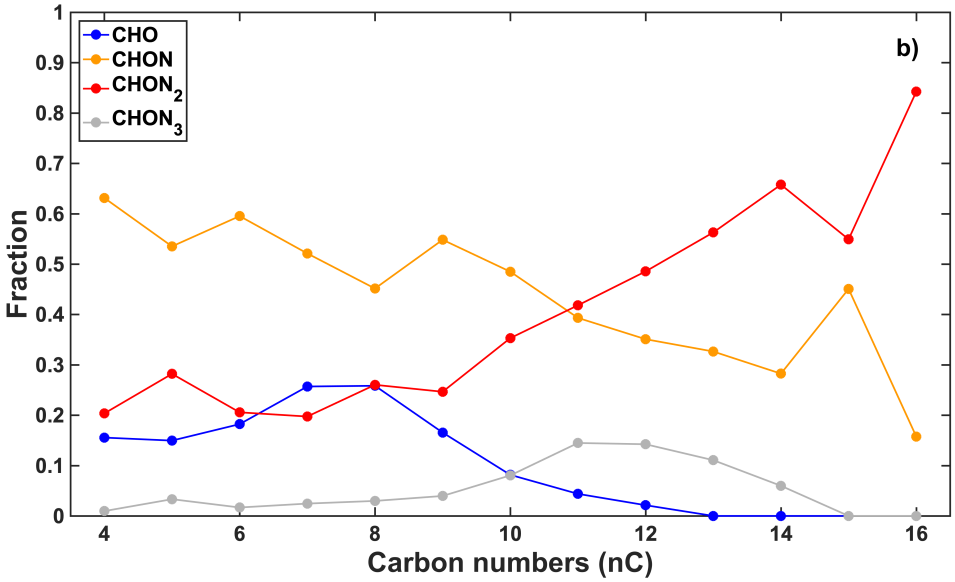

Figure 1b

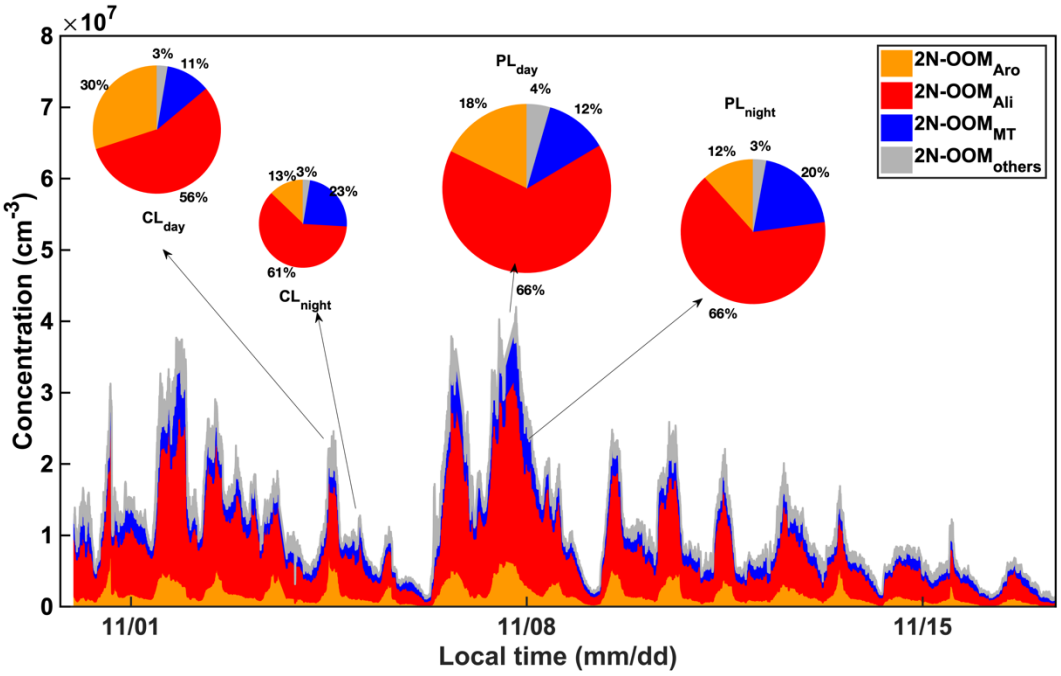

Figure 2

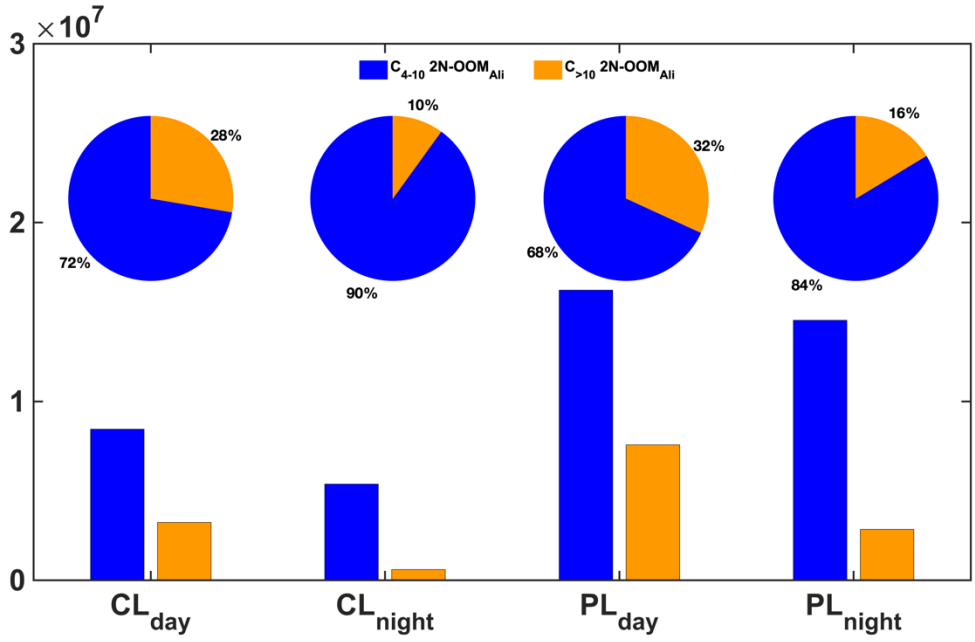

Figure 3

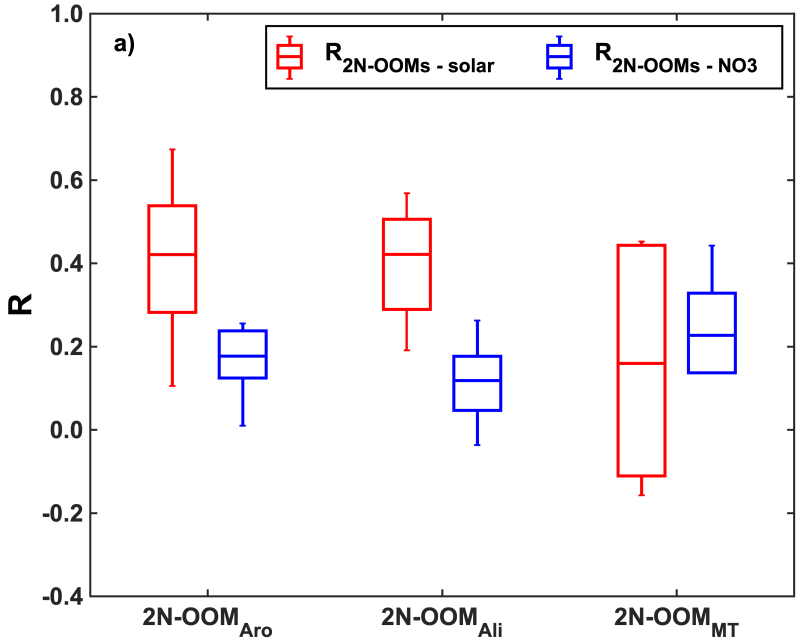

Figure 4a

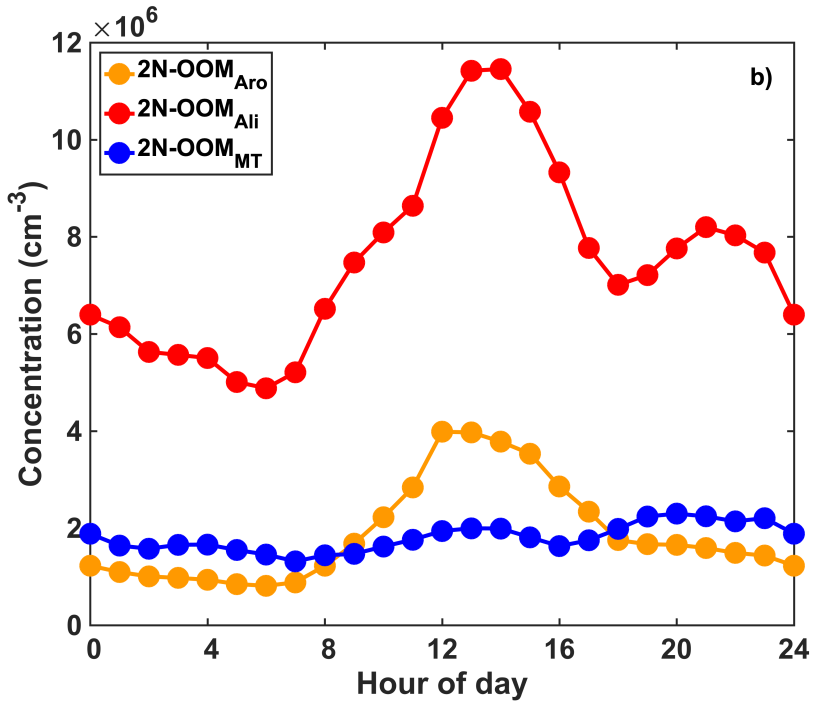

Figure 4b

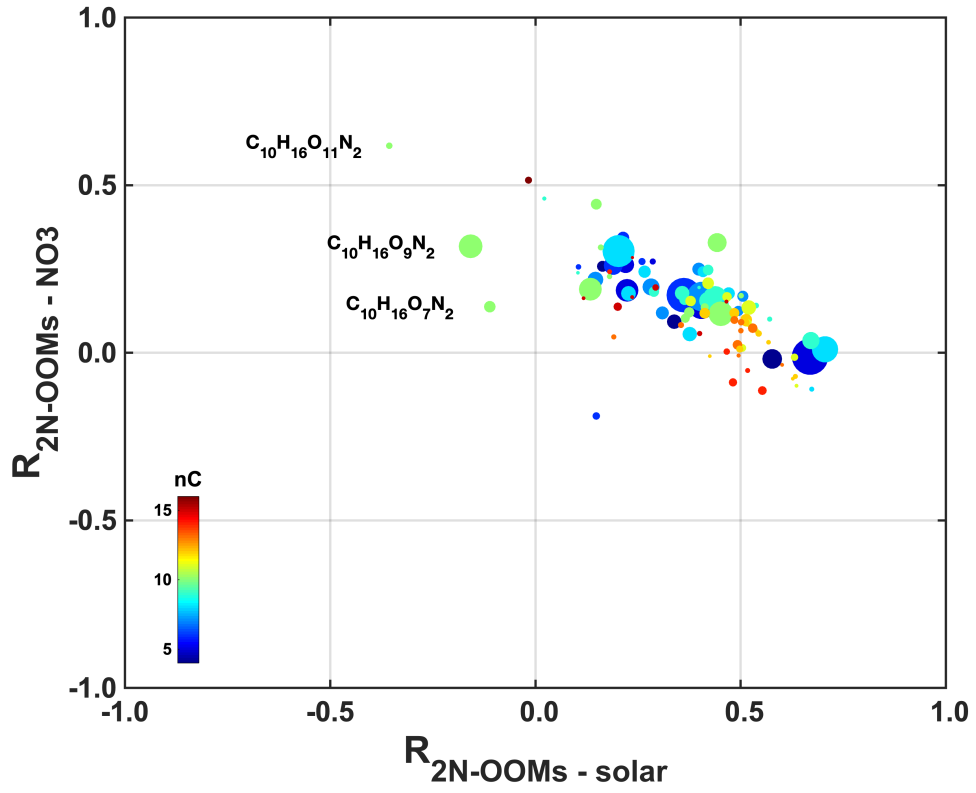

Figure 5

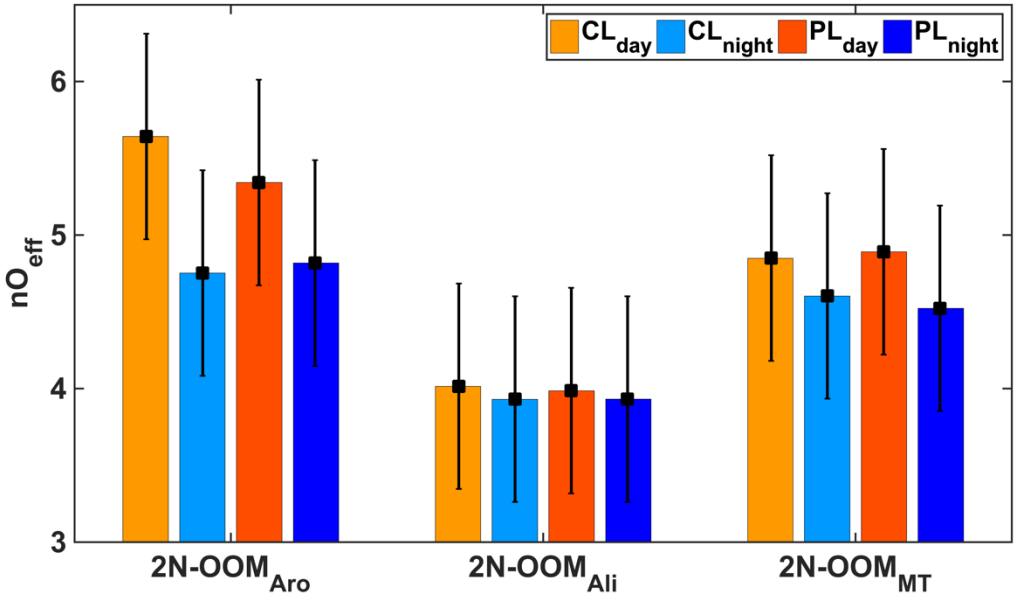

Figure 6

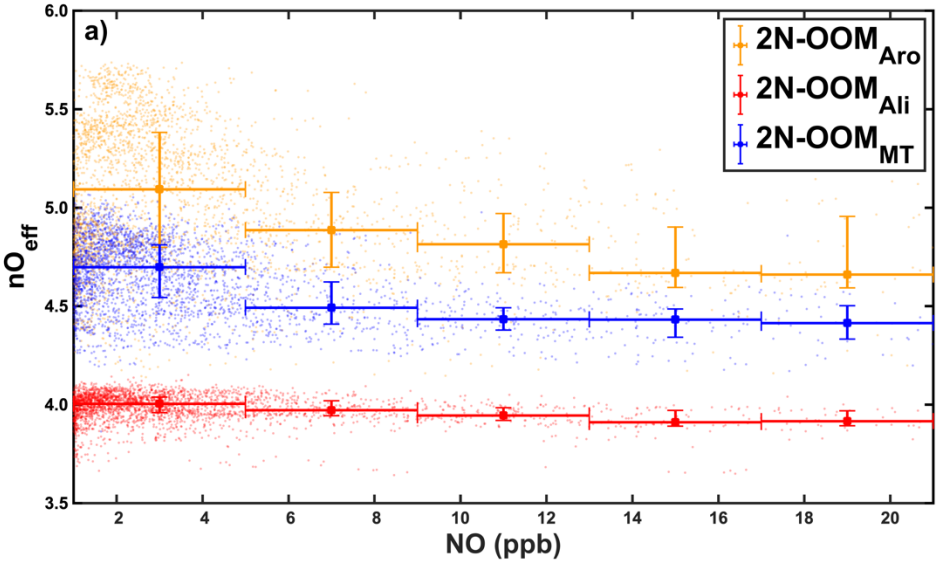

Figure 7a

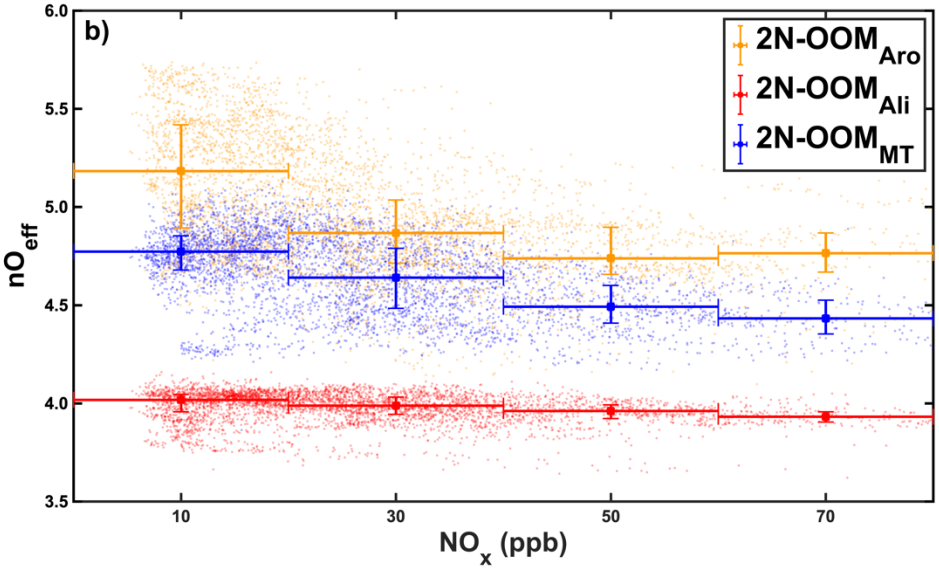

Figure 7b

Unambiguous identification of N-containing oxygenated organic molecules using CI-Orbitrap in an eastern Chinese megacity

Yiqun Lu[1,2], Yingge Ma[1], Dan Dan Huang[1], Shengrong Lou[1], Sheng'ao Jing[1], Yaqin Gao[1], Hongli Wang[1], Yanjun Zhang[3], Hui Chen[4], Yunhua Chang[5], Naiqiang Yan[2], Jianmin Chen[4], Christian George[3], Matthieu Riva[3], Cheng Huang[1]*

[1] State Environmental Protection Key Laboratory of Formation and Prevention of Urban Air Pollution Complex, Shanghai Academy of Environmental Sciences, Shanghai 200233, China;

[2] School of Environmental Science and Engineering, Shanghai Jiao Tong University, Shanghai 200240, China

[3] Univ. Lyon, Université Claude Bernard Lyon1, CNRS, IRCELYON, 69626 Villeurbanne, France;

[4] Shanghai Key Laboratory of Atmospheric Particle Pollution and Prevention (LAP[3]), Department of Environmental Science & Engineering, Jiangwan Campus, Fudan University, Shanghai 200438, China

[5] Collaborative Innovation Center on Forecast and Evaluation of Meteorological Disasters (CIC-FEMD), NUIST Center on Atmospheric Environment, Nanjing University of Information Science and Technology, Nanjing 210044, China

Contents of this file

Figure S5. Diel variation patterns of factors in 2-6 factor solutions of PMF. The panels from top to bottom are 2-factor solution, 3-factor solution, 4-factor solution, 5-factor solution and 6-factor solution, respectively.

Figure S6. The factor profiles in the six-factor solution.

Figure S7. The relative contributions of OOMs with different carbons to the extremely low-volatility organic compounds (ELVOC, $C^* < 3 \times 10^{-5}$ μg m^{-3}) and low-volatility organic compounds (LVOC, $3 \times 10^{-5} \leq C^* < 3 \times 10^{-1}$ μg m^{-3}).

Figure S8. Timeseries of N_2O_5 concentration (top panel), estimated NO_3 concentration (middle panel), and the nighttime factor-1 (bottom panel).

Figure S9. Timeseries of $PM_{2.5}$ concentration (top panel), and the episode factor-1 (bottom panel).

S1. Other ancillary measurements

The mass concentration of ambient particles was measured by particle monitor (TEOM 1405DF, Thermo, USA). SO_2, O_3 and NO_x concentrations were measured using a SO_2 analyzer (Model 43i, Thermo, USA), a O_3 analyzer (Model 49i, Thermo, USA) and a NO_x analyzer (Model 42i, Thermo, USA) with the detection limits of 0.1 ppbv, 0.5 ppbv and 0.4 ppbv, respectively. The above instruments were pre-calibrated before the campaign. The solar radiation was measured on the rooftop of the building. Atmospheric N_2O_5 concentrations were measured by an iodide CI-API-TOF. The concentrations of NO_3 radicals were estimated under the assumption that NO_3, NO_2 and N_2O_5 could reach an equilibrium quickly in tropospheric conditions (Brown and Stutz, 2012). The total concentrations of VOC precursors (TVOC) were determined by the measurement of an online GC-MS (7890A-5975C, Agilent, USA).

S2. Overview of the campaign

An overview of the measurement data, illustrating the air quality as well as the meteorological conditions (global radiation, temperature, wind direction, wind speed, and RH), concentrations of trace gases and pollutants ($PM_{2.5}$, O_3, NO_x, N_2O_5, and TVOCs) during the campaign, is provided in this section as shown in Figure S2 and Table S1. Firstly, the maximum intensities of global radiation on individual days were in a range of 637-867 W m^{-2}, indicating strong photochemical activities during the daytime of the campaign. The relative humidity (RH) exhibited a clear diurnal variation pattern with a range of 21-91% . The wind (0-7 m/s) from the north to northeast prevailed during the campaign and frequently resulted in increased $PM_{2.5}$ concentrations due to the transport. The $PM_{2.5}$ concentration were in a range of 6-59 μg m^{-3} (5-95 % percentile). The 5-95 % percentile ranges of [O_3], [NO_x], and [TVOC] were 4.6-58.6 ppbv, 8.9-69.6 ppbv, and 15.2-77.5 ppbv, respectively. O_3 showed an obvious diurnal variation, peaking at 13:00 – 15:00. Diurnal variations of NO_x and TVOC showed high concentrations over the rush hours. A PM episode with mean $PM_{2.5}$ concentration of 56.4 μg m^{-3} occurred from November 6th to November 8th, accompanied by a high concentration of both TVOC and NO_x, indicating the same origins

of air pollutants. While the N_2O_5 remained in low concentration levels in general, three peak concentrations up to about 600 pptv appeared at nighttime during November 6^{th}-8^{th}.

S3. Positive matrix factorization (PMF)

Positive matrix factorization (PMF) allows for time-resolved mass spectra to be expressed as a linear combination of a finite number of factors, assuming that the factor profiles are constant and unique. Since this method does not require a priori information about the factors, it is an ideal technique for extracting information from ambient measurements where the detailed chemistry, sources, and atmospheric processes are complex. PMF has already been used in source apportionment analysis of OOMs in previous studies (Yan et al., 2016; Zhang et al., 2019, 2022). In this study, PMF was performed using the Igor-based interface Source Finder (SoFi, v6.3), run by the multilinear engine (ME-2) (Canonaco et al., 2013). The data for the PMF model inputs were prepared according to the method described in previous studies (Zhang et al., 2022). Note that the orbitrap analyzer does not measure signal below a certain threshold resulting in incomplete time series for species present at low concentration level. Therefore, the species characterized by incomplete time series with more than 90% missing data and the spectra with more than 80% missing were removed (Zhang et al., 2022).

PMF analysis in this work was performed in 2-10 factors as shown in Figure S3. Five runs for each solution show good consistencies in both Q/Qexp and explained variation, indicating the small model uncertainty. The change of Q/Q_{exp}, which decreases stepwise from 2.61 (assuming two factors) to 0.65 (assuming nine factors). Since the absolute value of Q/Q_{exp} might be misleading, the trend of Q/Q_{exp} is useful to determine the minimum factor number (Ulbrich et al., 2009), a large decrease in Q/Q_{exp} indicates that the additional factor may explain a large fraction of unaccounted variability in the data. The third factor significantly decreases the Q/Qexp value from 2.61 to 1.83, suggesting the importance of the third factor. By adding the third factor, the model can explain 79.4 % of the data variation, in comparison to 75.4 % when only two factors are assumed. This improvement in model performance also implies the addition of third factor is crucial. The second largest increase in the explained fraction (from 79.4 % to 81.3 %) happens when adding the fourth factor and the Q/Qexp value decreases from 1.83 to 1.51. When

model contains 5, 6, 7, 8, 9 and 10 factors, the Q/Qexp values are about 1.27, 1.07, 0.94 and 0.83, 0.73 and 0.66 respectively while the explained fraction by mode are in a range of 82.9-87.5 %.

Since the PMF analysis is a pure mathematical method without any prior physical or chemical assumptions, choosing the best factor number is critical before describing the PMF results. In terms of trends, more factors would get more freedom to follow subtle variations of the matrix, however, artificially choosing too many factors will over analyze the matrix, resulting in the split of physically meaningful source apportionment into meaningless ones. The timeseries and diurnal variations of factors are shown in Figure S4 and Figure S5. The two-factor solution leads to a distinct daytime factor and a night factor. In the three-factor solution, the timeseries of first two factors are more or less the same as those in the two-factor case, but the variation pattern of second factor has changed in the daytime, the new factor tracks the $PM_{2.5}$ concentration well in two PM episodes, and exhibits a ush-hour peak in the morning. The four-factor solution results in two daytime factors originated from the old daytime factor. When five factors are assumed, an additional nighttime factor appears. When six factors are assumed, an afternoon rush-hour factor appears. For seven factors, the derived new factor has no strong correlation with any independent tracer. Herein, we concluded that the PMF solution with six factors is the optimal solutions and chose to limit our further analysis to the six-factor solution because it is not possible to distinguish the identification of "real" factors without significant correlations. The factor profiles in the six-factor solution could be seen in Figure S6.

In the aspect of variation patterns, we classify the six factors into three types. The first two factors are related to the daytime photochemical activities and defined as daytime factor-1 and daytime factor-2. The third factor and fourth factor show clear nocturnal patterns and defined as nighttime factor-1 and nighttime factor-2. The fifth factor and the sixth factor are more related to the emission episode and thus defined as episode factor-1 and episode factor-2. Table S1 shows the peak times and fingerprint molecules of the factors.

Figure S1. The map of the field site (Shanghai Academy of Environmental Sciences) that is a representative urban station.

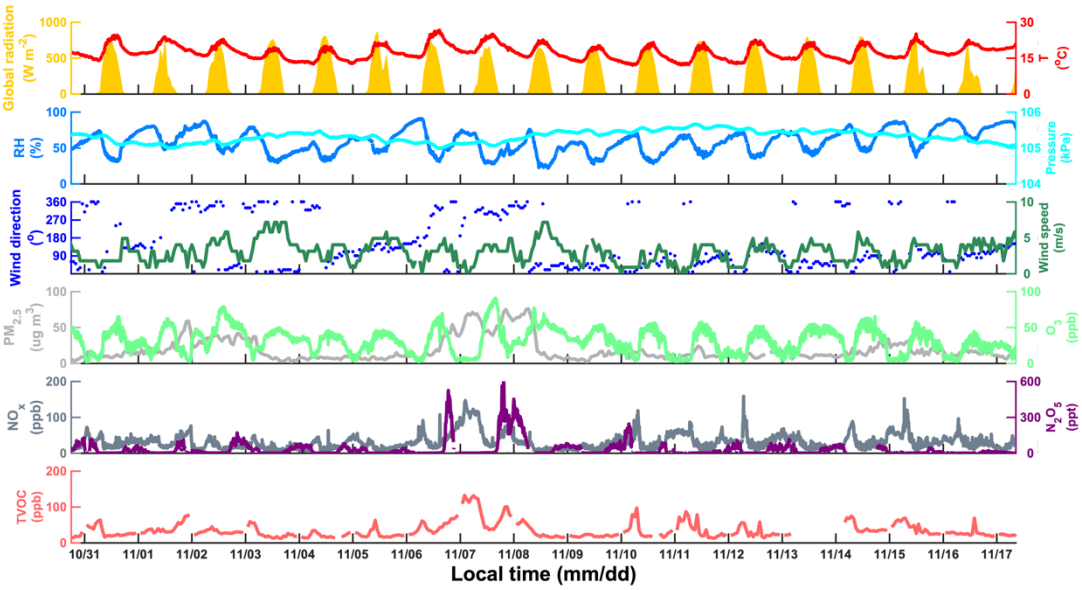

Figure S2. Timeseries of key measurements during the field campaign.

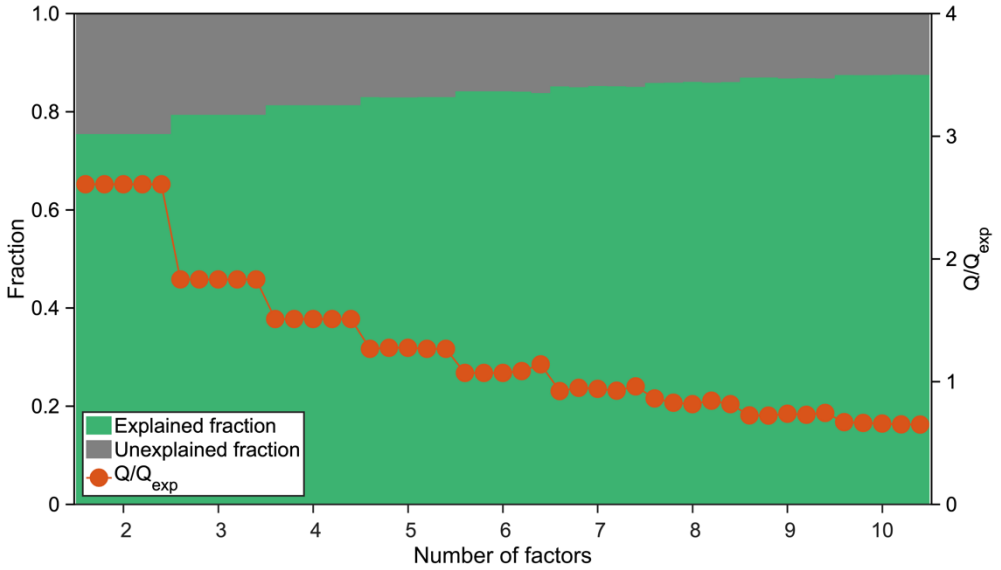

Figure S3. Mathematical diagnostics of PMF solutions, including the overall changes of Q/Qexp and the explained variation from two-factor to nine-factor solutions. For each number of factors, five seed runs were performed to test the consistency of the solution.

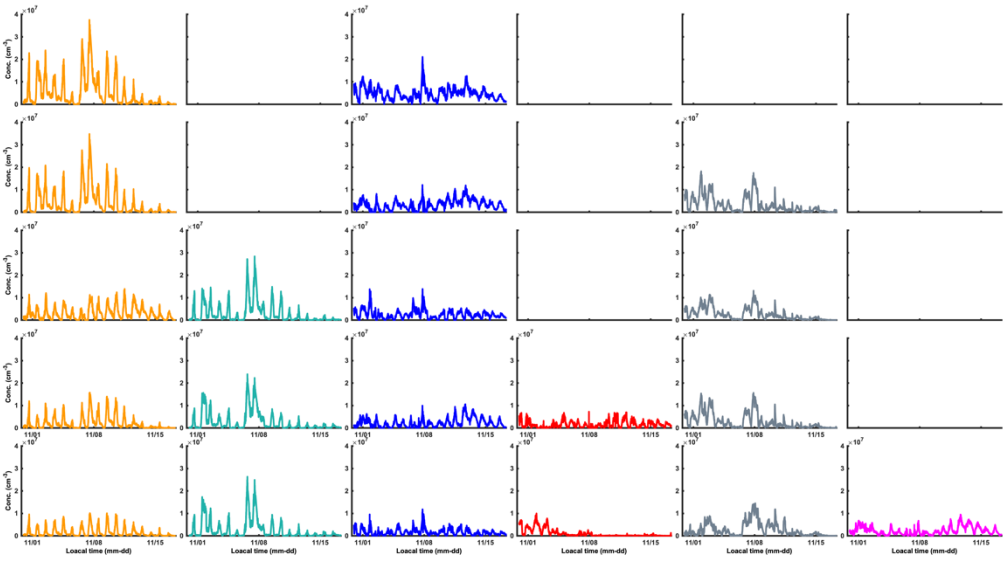

Figure S4. Timeseries of factors in 2-6 factor solutions of PMF. The panels from top to bottom are 2-factor solution, 3-factor solution, 4-factor solution, 5-factor solution and 6-factor solution, respectively.

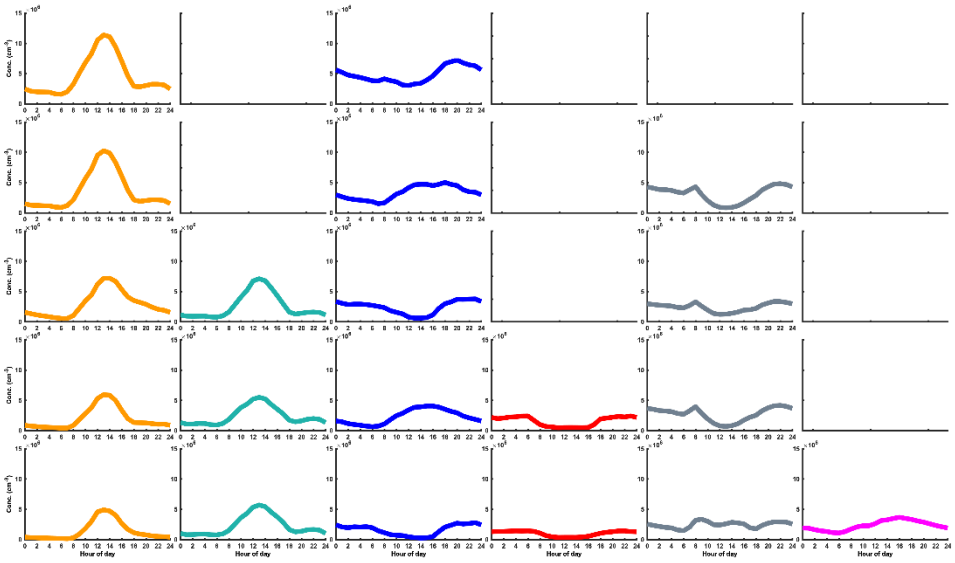

Figure S5. Diel variation patterns of factors in 2-6 factor solutions of PMF. The panels from top to bottom are 2-factor solution, 3-factor solution, 4-factor solution, 5-factor solution and 6-factor solution, respectively.

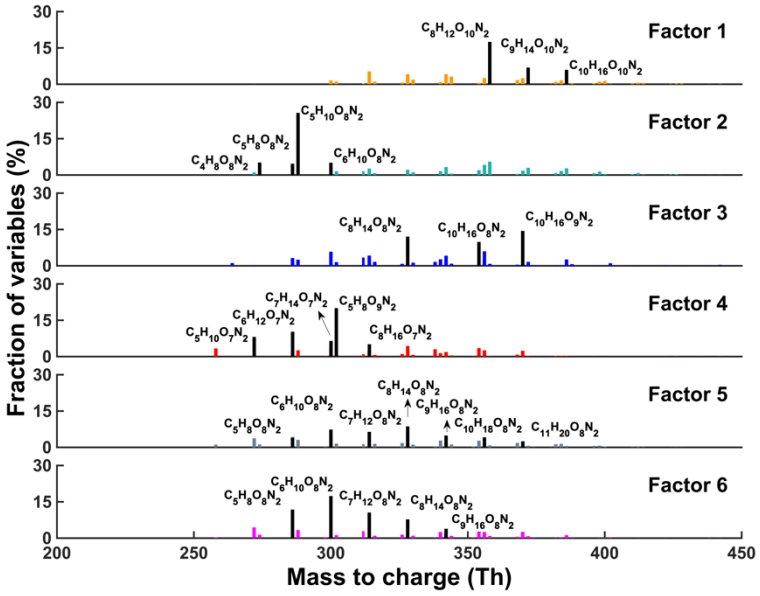

Figure S6. The factor profiles in the six-factor solution, the black ones represent fingerprint molecules.

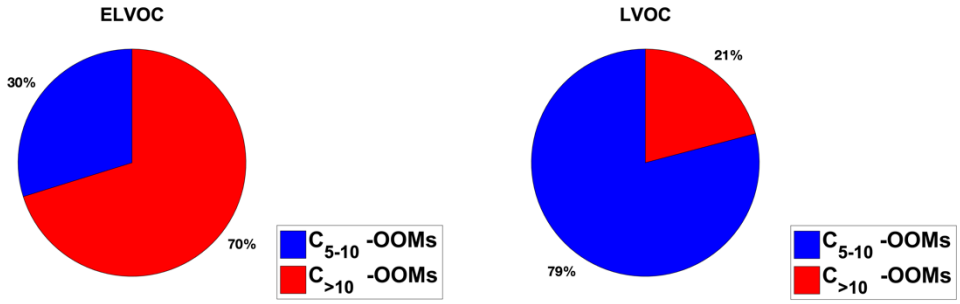

Figure S7. The relative contributions of OOMs with different carbons to the extremely low-volatility organic compounds (ELVOC, C* < 3 × 10^{-5} μg m^{-3}) and low-volatility organic compounds (LVOC, 3 × 10^{-5} ≤ C* < 3 × 10^{-1} μg m^{-3}).

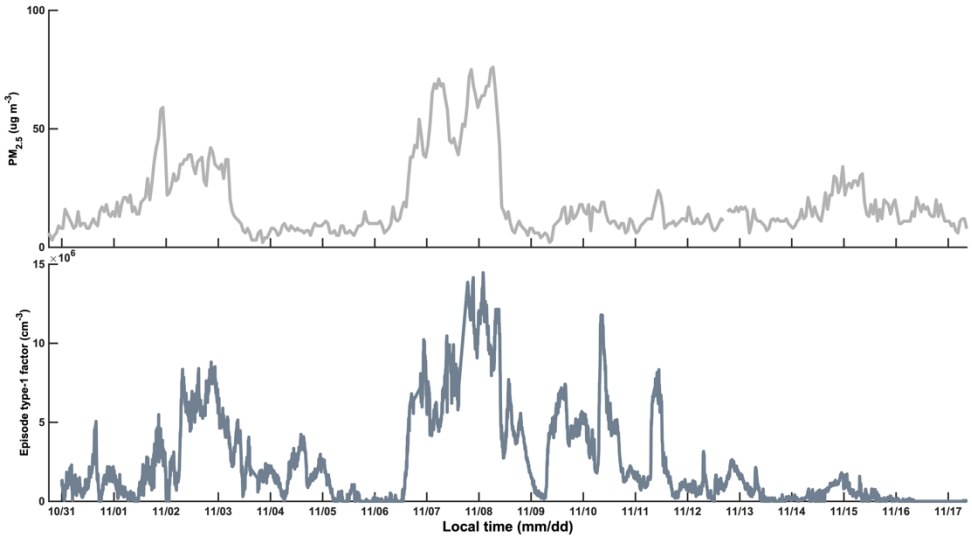

Figure S8. Timeseries of $PM_{2.5}$ concentration (top panel), and the episode factor-1 (bottom panel).

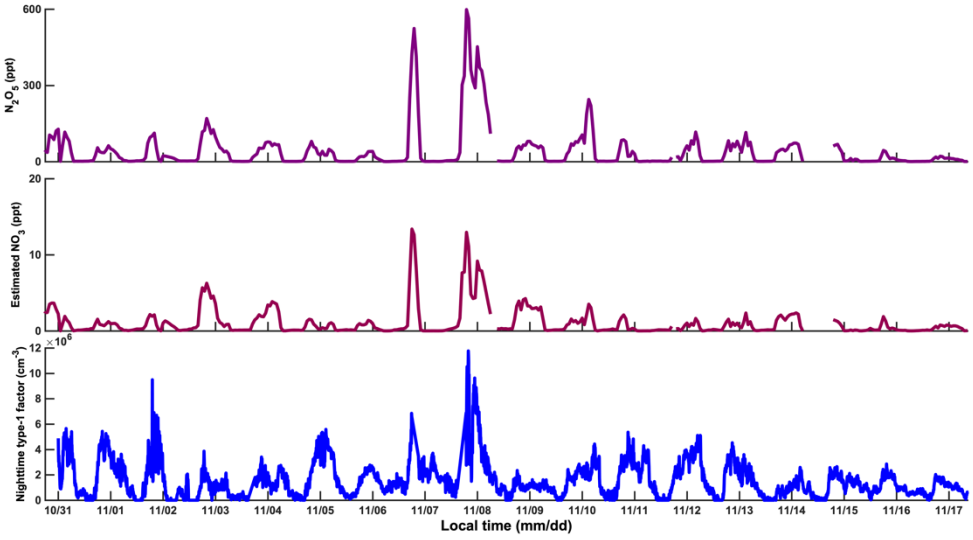

Figure S9. Timeseries of N_2O_5 concentration (top panel), estimated NO_3 concentration (middle panel), and the nighttime factor-1 (bottom panel).

Table S1 Summary of the Factors in six-factor solution

Factor	Factor	Peak time	Fingerprint molecules
Daytime	Daytime factor-1	12:00-14:00	$C_nH_{2n-4}O_{10}N_2$ (n=8-10)
	Daytime factor-2	12:00-14:00	$C_nH_{2n}O_8N_2$ (n=4-5), $C_nH_{2n-2}O_8N_2$ (n=5-6)
Nighttime	Nighttime factor-1	19:00-23:00	$C_{10}H_{16}O_9N_2$, $C_{10}H_{16}O_8N_2$, $C_8H_{14}O_8N_2$
	Nighttime factor-2	20:00-06:00	$C_5H_8O_9N_2$, $C_nH_{2n}O_7N_2$ (n=5-8)
Episode	Episode factor-1	PM episode	$C_nH_{2n-2}O_8N_2$ (n=5-11)
	Episode factor-2	Afternoon rush-hour (16:00)	$C_nH_{2n-2}O_8N_2$ (n=5-9)

Table S2 Averaged nO_{eff} of 2N-OOMs in the four cases

Case	$\overline{[2N-OOM_{Aro}]}$	$\overline{[2N-OOM_{Ali}]}$	$\overline{[2N-OOM_{MT}]}$	$\overline{[2N-OOM_{Total}]}$
CL_{day}	5.6	4.0	4.8	4.6
CL_{night}	4.8	3.9	4.6	4.2
PL_{day}	5.3	4.0	4.9	4.3
PL_{night}	4.8	3.9	4.5	4.1

Reference

Brown, S. S. and Stutz, J.: Nighttime radical observations and chemistry, Chem. Soc. Rev., 41, 6405–6447, doi:10.1039/c2cs35181a, 2012.

Canonaco, F., Crippa, M., Slowik, J. G., Baltensperger, U. and Prévôt, A. S. H. H.: SoFi, an IGOR-based interface for the efficient use of the generalized multilinear engine (ME-2) for the source apportionment: ME-2 application to aerosol mass spectrometer data, Atmos. Meas. Tech., 6(12), 3649–3661, doi:10.5194/amt-6-3649-2013, 2013.

Ulbrich, I. M., Canagaratna, M. R., Zhang, Q., Worsnop, D. R. and Jimenez, J. L.: Interpretation of organic components from Positive Matrix Factorization of aerosol mass spectrometric data, Atmos. Chem. Phys., 9(9), 2891–2918, doi:10.5194/acp-9-2891-2009, 2009.

Yan, C., Nie, W., Äijälä, M., Rissanen, M. P., Canagaratna, M. R., Massoli, P., Junninen, H., Jokinen, T., Sarnela, N., Häme, S. A. K., Schobesberger, S., Canonaco, F., Yao, L., Prévôt, A. S. H., Petäjä, T., Kulmala, M., Sipilä, M., Worsnop, D. R. and Ehn, M.: Source characterization of highly oxidized multifunctional compounds in a boreal forest environment using positive matrix factorization, Atmos. Chem. Phys., 16, 12715–12731, doi:10.5194/acp-16-12715-2016, 2016.

Zhang, Y., Peräkylä, O., Yan, C., Heikkinen, L., Äijälä, M., Daellenbach, K. R., Zha, Q., Riva, M., Garmash, O., Junninen, H., Paatero, P., Worsnop, D. and Ehn, M.: A novel approach for simple statistical analysis of high-resolution mass spectra, Atmos. Meas. Tech., 12(7), 3761–3776, doi:10.5194/amt-12-3761-2019, 2019.

Zhang, Y., Li, D., Ma, Y., Dubois, C., Wang, X., Perrier, S., Chen, H., Wang, H., Jing, S., Lu, Y., Lou, S., Yan, C., Nie, W., Chen, J., Huang, C., George, C. and Riva, M.: Field Detection of Highly Oxygenated Organic Molecules in Shanghai by Chemical Ionization–Orbitrap, Environ. Sci. Technol., doi:10.1021/acs.est.1c08346, 2022.